Прилози, Одд. мат. тех. науки, МАНУ, XXVI, 1 (2005), с. 7–84
Contributions, Sec. Math. Tech. Sci., MANU, XXVI, 1 (2005), pp. 7–84
ISSN 0351–3246
UDC: 549.06:543.422.4(497.7)

Review paper

MINERALS FROM MACEDONIA. COMPLEMENTARY USE OF VIBRATIONAL SPECTROSCOPY AND POWDER X-RAY DIFFRACTION FOR IDENTIFICATION AND DETECTION PURPOSES

Gligor Jovanovski, Petre Makreski, Bojan Šoptrajanov
Branko Kaitner, Blažo Boev

A b s t r a c t: A review of the results of complementary use of vibrational spectroscopy (infrared and Raman) and powder X-ray diffraction in the process of identification and detection of some carbonate, sulfide, oxide and silicate minerals originating from the Republic of Macedonia is presented. Studied are the following minerals: calcite, $CaCO_3$; aragonite, $CaCO_3$; siderite, $FeCO_3$; magnesite, $MgCO_3$; dolomite, $CaMg(CO_3)_2$; kutnahorite, $CaMn(CO_3)_2$; galena, PbS; sphalerite/wurtzite, (Zn,Fe)S; hematite, Fe_2O_3; magnetite, Fe_3O_4; limonite, FeOOH; goethite, α-FeOOH; corundum, Al_2O_3; rutile, TiO_2; chromite, $FeCr_2O_4$; almandine, $Fe_3Al_2(SiO_4)_3$; spessartine, $Mn_3Al_2(SiO_4)_3$; zircon, $ZrSiO_4$; titanite, $CaTiSiO_5$; olivine, $(Mg,Fe)_2SiO_4$; forsterite, Mg_2SiO_4; staurolite, $Fe_2Al_9O_6(SiO_4)_4(OH)_2$; kyanite, Al_2SiO_5.

Key words: minerals; vibrational spectroscopy; powder X-ray diffraction

1. INTRODUCTION

The Republic of Macedonia is very rich in minerals. It lies in the Alpine–Balkan–Carpathian–Dinaride collision belt and a large number of carbonate, sulfide, oxide, silicate and other types of ore deposits are present in Macedonia. For instance, there is a unique ore deposit at Alšar (near Kavadarci) where 44 mineral species have been identified up to now.

In spite of these very rich ore deposits in a relatively small area, the total number of minerals present in Macedonia is not yet fully established. There

are a few incomplete mineral collections, but no complete literature data concerning their systematizaton and characterization are available. In order to prepare the *Atlas of Minerals from Macedonia* (a task presently in hand), the systematic process of collection, separation, identification and systematization as well as spectroscopic and structural characterization of minerals originating from Macedonia was undertaken.

The acquisition of all the available minerals is almost completed and the *Mineral Collection* at the Institute of Chemistry in Skopje is set up. The minerals are studied mainly by Fourier transform infrared and Raman vibrational spectroscopy and by powder X-ray diffraction [1–23]. In order to determine the presence and content of trace elements in the minerals, atomic absorption spectrometry and inductively coupled plasma – atomic emission spectrometry are also used and analytical methods for discrimination between some mineral species are developed [e.g. 24–39]. It should be noted here that various instrumental techniques and procedures for mineral detection, identification, discrimination and quantitative determination have been developed during the last few decades. The most frequently used among them are X-ray diffraction [40], vibrational infrared [41] and Raman [42] spectroscopy, thermal analysis [43] and optical diffuse reflectance [44] (only a selection of the relevant references is given above).

Here a review of the results of the complementary use of vibrational spectroscopy (infrared and Raman) and powder X-ray diffraction in the process of identification and detection of some carbonate, sulfide, oxide and silicate minerals originating from the Republic of Macedonia is presented. The identification is based on the comparison of the results of our study with the corresponding literature data for the analogous mineral species originating from other localities in the world. It is worth mentioning that, in general, the comparison of the data is often accompanied by difficulties, the most important among them being related to the temperature at which the experiment was performed; the instrument resolution; the vibrational spectral region and/or 2θ region of the registered powder X-ray patterns; the specimen quantity used in the experiment; the sample preparation, particle size and shape; the locality where the specimen was collected from, etc.

2. EXPERIMENTAL

The studied minerals were collected from various localities (Fig. 1). After that, from the collected ore samples single crystals were carefully picked up under a microscope and then powdered.

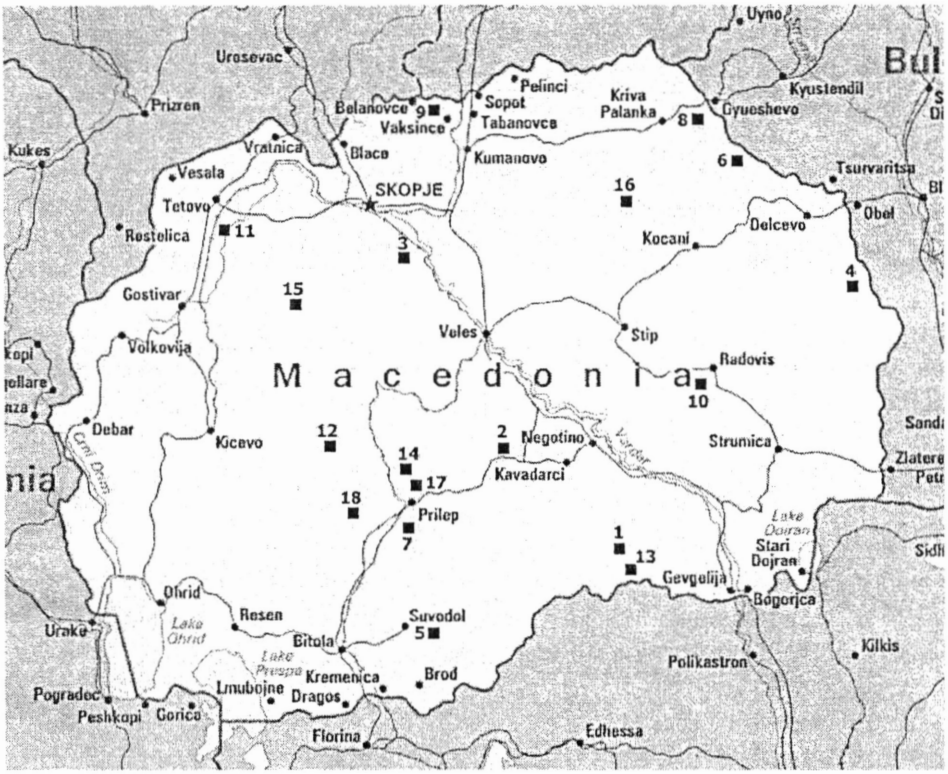

Fig. 1. The localities of the studied minerals: 1) 'Ržanovo (aragonite, hematite, olivine), 2) Mrzen (calcite), 3) Pčinja (magnezite), 4) Pehčevo (limonite), 5) Dunje (titanite), 6) Sasa (kutnahorite, galena, sphalerite), 7) Štavica (kyanite, staurolite), 8) Toranica (sphalerite), 9) Lojane (spessartine), 10) Damjan (hematite, magnetite), 11) Raduša (chromite), 12) Košino (magnetite), 13) Alšar (goethite), 14) Pelagon (almandine), 15) Kozjak (zircon), 16) Zletovo (siderite, galena, sphalerite), 17) Sivec (calcite, corundum, dolomite), 18) Veselčani (rutile)

The far infrared spectra of the studied samples were recorded on a Bruker 113 v FT IR interferometer, whereas a Perkin-Elmer FT IR system 2000 interferometer was employed for the spectra in the mid-IR region. In the former case, mulls in Nujol between polyethylene plates were prepared, whereas the KBr pellet method was used for the mid-infrared spectra.

The Raman spectra of the studied mineral samples were recorded on three instruments: a Jobin Yvon LabRam Infinity spectrometer with 532 nm laser line of an Nd-YAG frequency-double laser; a Bruker FT Raman model

106/S connected to FT IR interferometer Equinox 55 with 1064 nm line of Nd-YAG frequency laser; a Renishaw micro-Raman 1000 spectrometer equipped with a Peltier cooled CCD camera and Leica microscope for sample illumination with 50 × magnification and numerical aperture of 0.75, the Raman effect being excited using the 514 nm line of an air cooled Ar^+ laser by Melles Griot.

The measurements were conducted at a room temperature and spectral data were analyzed with the GRAMS/32 software package.

A Philips Analytical X-ray diffractometer PW 3710 was used for X-ray powder diffraction. A generator with 50 kV and electricity of 30 mA was employed as a source for Cu$K\alpha$ radiation.

3. RESULTS AND DISCUSSION

3.1. Carbonate mineral samples

Since carbonate minerals, especially the polymorphic forms of $CaCO_3$ (calcite and aragonite), may appear in common mineral aggregates, it is often advantageous to use rapid and simple methods for their distinction and identification as well as for detecting impurities in one another. Here some of the results of the use of FT IR spectroscopy [14, 16] and powder X-ray diffraction [6] in order to distinguish between the structurally different calcite and aragonite types of carbonate minerals, as well as to discriminate between the isomorphous rhombohedral carbonate minerals calcite, magnesite, siderite, dolomite and kutnahorite, will be presented. The detection of impurities in the corresponding carbonate mineral mixtures by both techniques will be discussed as well [6, 8, 14, 16].

Calcite and aragonite types

The discrimination between the calcite and aragonite type of carbonate minerals by infrared spectroscopy is a fairly easy task. Namely, due to the lower local symmetry of the CO_3^{2-} ions in the aragonite type minerals (C_s) compared to the calcite type (D_3), the FT IR spectra of the two polymorphic forms of $CaCO_3$ (calcite and aragonite) are rather different, as seen in Fig. 2 [14]. It leads to the appearance of the band due to the ν_1 mode (symmetric CO_3^{2-} stretching) in the spectrum of aragonite (at 1083 cm^{-1}) and its isomorphous analogues (viterite, cerusite), which is absent in the spectrum of calcite

and its isomorphous analogues (siderite, magnesite, dolomite). Another noticeable difference between the two types of spectra is the appearance of two bands in the spectrum of aragonite (at 712 and 699 cm^{-1}) instead of one (at 712 cm^{-1}) in the spectrum of calcite in the region of the in-plane bending modes (ν_4). Rather pronounced frequency differences between the corresponding ν_3 (antisymmetric stretching) and ν_2 (out-of-plane bending) modes in both spectra are observed as well (see Fig. 2).

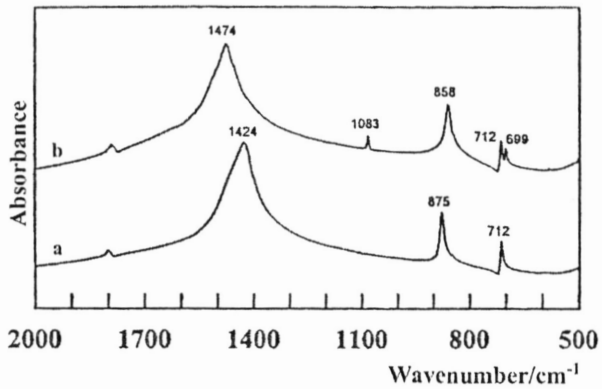

Fig. 2. The FT IR spectra of calcite (Sivec) (a) and aragonite ('Ržanovo) (b)

The discrimination between the rhombohedral calcite and the orthorhombic aragonite by powder X-ray diffraction is an even easier task compared to the use of FT IR spectroscopy. Namely, the X-ray patterns of these two polymorphic forms of $CaCO_3$ are quite different [6].

The above-mentioned differences between the FT IR spectra of the structurally different calcite and aragonite as well as between their powder X-ray patterns were used [6, 8, 14] for detecting their impurities in one another.

Like other methods, the detection of mineral impurities by IR spectroscopy is based on the presence of analytical bands in the regions where there are no absorption bands from the major constituent of the studied system. It is the appearance of the ν_1 mode (1083 cm^{-1}) in the spectrum of aragonite (absent in calcite spectrum), which made it possible [14] to detect the presence of small amounts of aragonite in calcite (Fig. 3). As seen in Fig. 3, the lower limit of detection of aragonite in calcite amounts to $\approx$ 1 wt %.

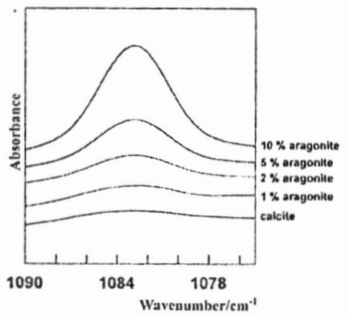

Fig. 3. The FT IR spectra of calcite (from Sivec) and mixtures of calcite with aragonite (from 'Ržanovo)

In ref. [14] it is also shown that the X-ray diffraction technique makes it possible to discriminate between any minerals from the calcite group (for example, siderite) and aragonite. Namely, the powder X-ray diagrams of siderite (Fig. 4a) and aragonite (Fig. 4b) show that the appearance of rather intense diffraction maximum at $2\theta = 27.620\,^{\circ}$ in the aragonite Debye diagram (absent in the siderite one) as well as the existence of a very strong maximum at $2\theta = 31.970\,^{\circ}$ in the siderite diagram (where aragonite does not exhibit diffraction) enables detection of impurities of aragonite in siderite and vice versa. The analysis showed that the limit of detection of impurities of aragonite in siderite by powder X-ray diffraction was around 1 wt % (Fig. 5), whereas the lower limit of detection of aragonite in siderite was about 0.5 wt % (Fig. 6).

The comparison of the obtained data regarding the determination of the impurities of siderite present in aragonite and vice versa showed that, in the current case, the powder X-ray diffraction is more accurate than the infrared spectroscopy, but this should not be used as a general conclusion, because the determination of the low limit of the present impurities varies from case to case.

FT IR spectroscopy can be even used in order to discriminate between the calcite group (calcite, $CaCO_3$; magnesite, $MgCO_3$; siderite, $FeCO_3$) as well as the dolomite group (dolomite, $CaMg(CO_3)_2$; kutnahorite, $CaMn(CO_3)_2$) of rhombohedral carbonate minerals [16]. Although both groups of above-mentioned minerals share essentially the same structure and are collectively called *rhombohedral carbonates* (Table 1), significant frequency differences between the corresponding ν_3, ν_2 and, especially, ν_4 active modes in their FT IR spectra were observed (Fig. 7, Table 2). These are mainly due to the rather marked sensitivity of the ν_4 vibrational mode (Table 2) to the change of the divalent-cation size [$r(Ca^{2+}) > r(Fe^{2+}) > r(Mg^{2+})$] [16] (Table 1).

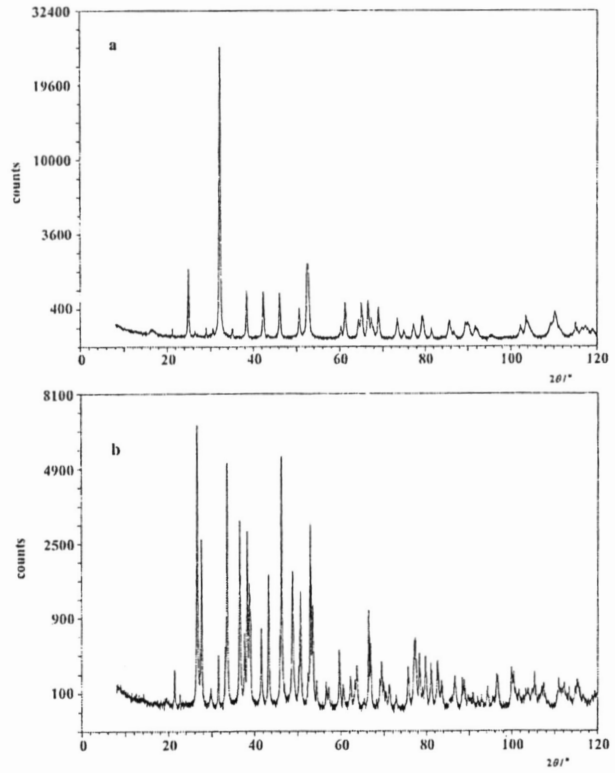

Fig. 4. Powder X-ray patterns of siderite from Zletovo (a) and aragonite from 'Ržanovo (b)

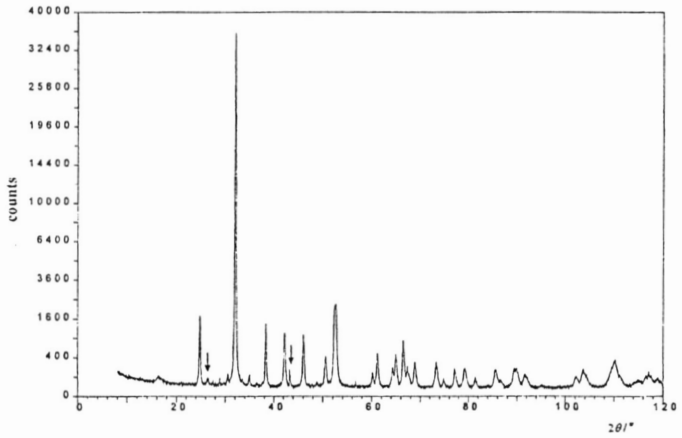

Fig. 5. Powder X-ray patterns of mineral mixture containing 99 % siderite and 1 % aragonite. The aragonite maxima are denoted by arrows

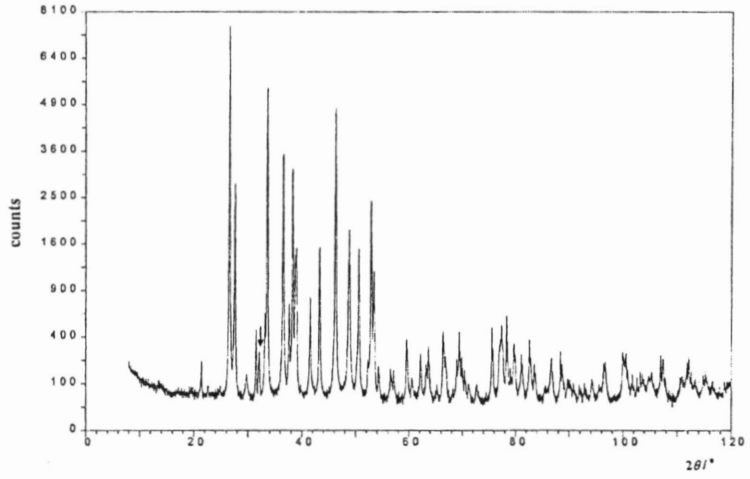

Fig. 6. Powder X-ray patterns of mineral mixture containing 99 % aragonite and 1 % siderite. The siderite maximum is denoted by an arrow

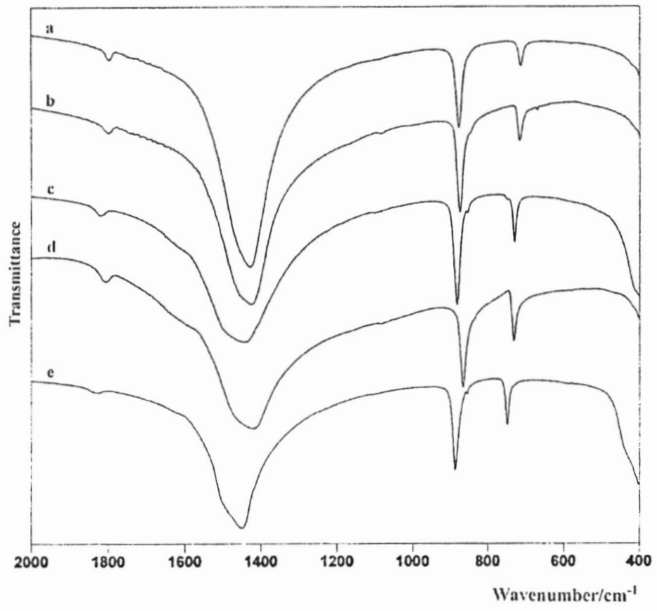

Fig. 7. FT IR spectra of the studied rhombohedral carbonates: calcite from Mrzen (a), kutnahorite from Sasa (b), dolomite from Prilep (c), siderite from Zletovo (d) and magnesite from Pčinja (e)

Table 1

The most important crystallographic data for the studied rhombohedral carbonates [45]

Mineral	Crystal System	Space group	Unit cell parameters /Å	Unit cell volume /Å^3	Z	Cation properties	
						Ionic radii/Å	CN
Calcite, $CaCO_3$	Hexagonal (rhombohedral)	$R\bar{3}c$	$a = 4.99$ $c = 17.06$	367.9	6	1.00	6
Siderite, $FeCO_3$	Hexagonal (rhombohedral)	$R\bar{3}c$	$a = 4.69$ $c = 15.38$	293.0	6	0.78	6
Magnesite, $MgCO_3$	Hexagonal (rhombohedral)	$R\bar{3}c$	$a = 4.63$ $c = 15.01$	278.7	6	0.72	6
Kutnahorite, $CaMn(CO_3)_2$	Hexagonal (rhombohedral)	$R\bar{3}$	$a = 4.85$ $c = 16.34$	332.9	3	$(0.91)_{av}$	6
Dolomite, $CaMg(CO_3)_2$	Hexagonal (rhombohedral)	$R\bar{3}$	$a = 4.80$ $c = 15.98$	318.9	3	$(0.86)_{av}$	6

Table 2

The spectroscopic data of the studied rhombohedral carbonates

Mineral	Vibrational frequencies /cm^{-1}		
	ν_3	ν_2	ν_4
Calcite – $CaCO_3$	1427	876, 875[a]	712, 725[a]
Kutnahorite[b] – $CaMn(CO_3)_2$	1425	873	716
Dolomite – $CaMg(CO_3)_2$	1443	881	728
Siderite[c] – $FeCO_3$	1421	866	731
Magnesite – $MgCO_3$	1450	887	748

[a] Calcite sample from Damjan.
[b] Both kutnahorite species have the same frequency values.
[c] All three siderite species have the same frequency values.

The large frequency difference (of 36 cm^{-1}) between the corresponding ν_4 modes in the FT IR spectra of magnesite (748 cm^{-1}) and calcite (712 cm^{-1}) was used to detect the presence of about 1 wt % of calcite in magnesite (Fig. 8) and vice versa (Fig. 9).

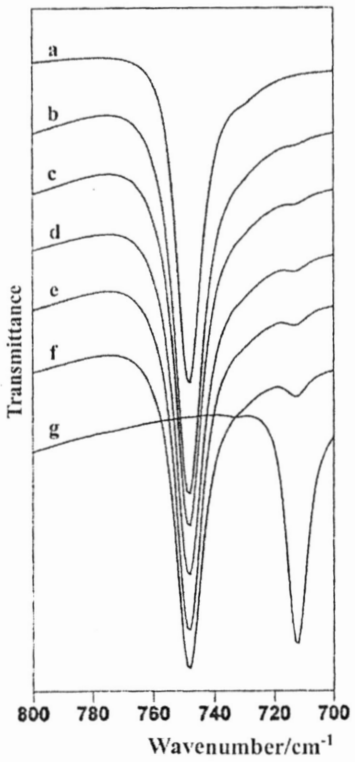

Fig. 8. FT IR spectra of magnesite (a) and calcite (g) and mixtures of 1, 2, 3, 5 and 10 wt % calcite in magnesite (b–f)

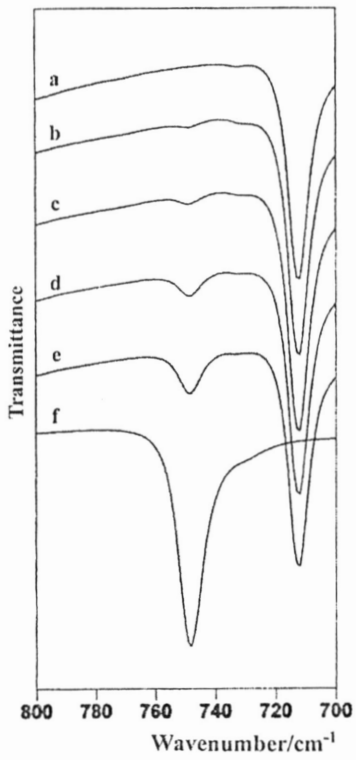

Fig. 9. FT IR spectra of calcite (a) and magnesite (f) and mixtures of 1, 2, 5 and 10 wt % magnesite in calcite (b–e)

3.2. Sulfide mineral samples

Numerous ore deposits are present in the Republic of Macedonia, the sulfide minerals being the commonly exploited reserves. The most attractive among the mineral species is lorandite, $Tl_2As_2S_4$, found in the Alšar ore deposit, and known as the best possible mineral detector for solar neutrinos [e.g. 46, 47].

Some of these sulfide minerals appear as a well-formed single crystal but more often they are accompanied by some other mineral forms. This, of course, gives rise to difficulties during their separation, identification and characterization some of which are listed below together with the results obtained in the course of the investigations.

Galena

The marked similarity between the FT IR spectra (Fig. 10) as well as the Raman spectra (Fig. 11) of four galena samples (two from Sasa and two from Zletovo) suggests that they belong to the same mineral species. Furthermore, the appearance of only one extremely wide, complex and intense band in the infrared spectrum of the four studied samples with the maximum ranging from 155 to 164 cm^{-1} (Fig. 10) is in agreement with the corresponding data found in the literature [48–50].

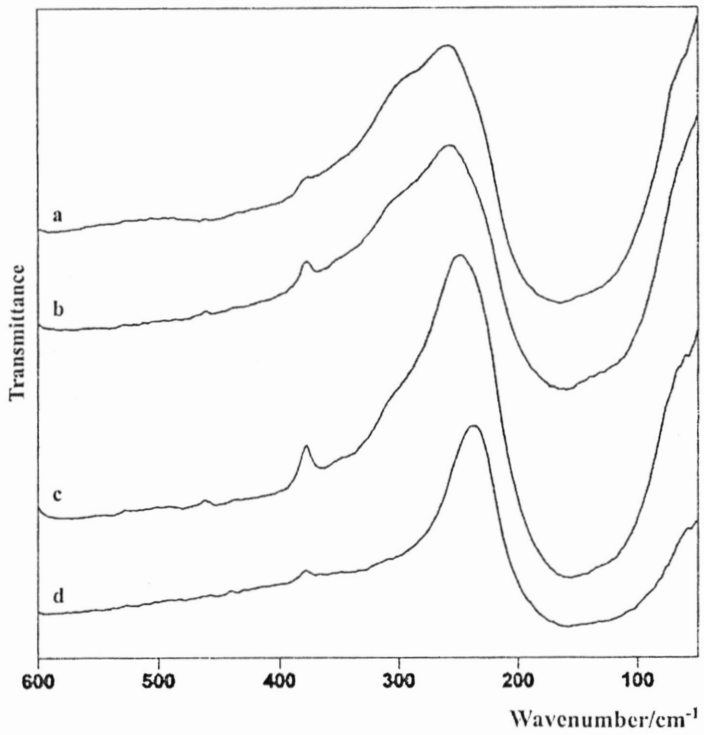

Fig. 10. The FT IR spectra of galena from Zletovo (a, d) and Sasa (b, c)

However, although, according to the group theory [49], no first-order Raman bands are expected in the galena spectrum, additional weak bands were observed (around 265 and 425 cm^{-1}) in the Raman spectra studied by us [10, 13] (Fig. 11). Their variable intensity indicates that they may be due to the

presence of some kind of impurities. On the other hand, the weak band at around 960 cm^{-1}, which appears in the Raman spectra of all studied galena samples with more or less the same intensity, may be regarded as an indication of the possible presence of a small amount of $PbSO_4$.

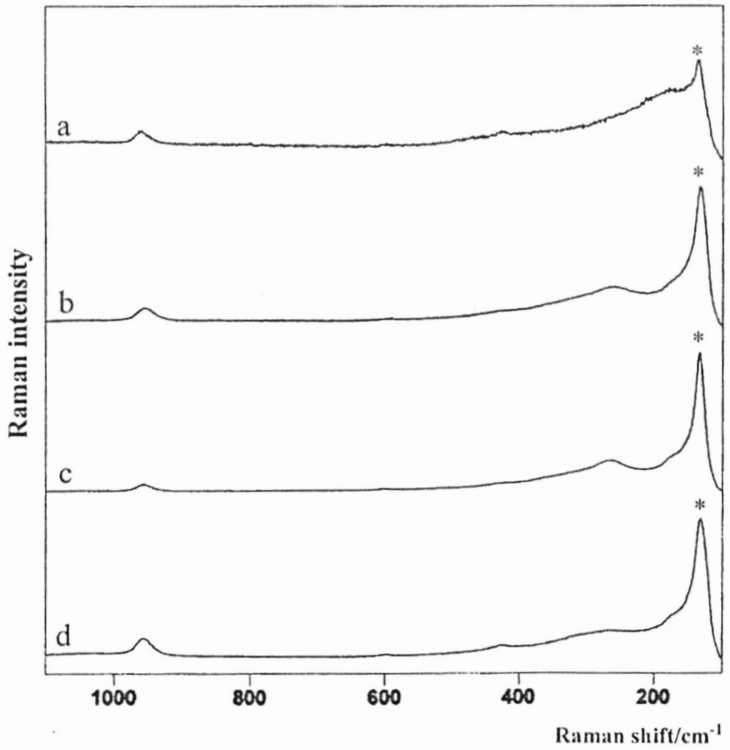

Fig. 11. The Raman spectra of galena from Zletovo (a, b) and Sasa (c, d) (* – "filter cut-out" from the Rayleigh line)

The identity between the powder X-ray diagrams of the studied galena samples from Sasa and from Zletovo (Fig. 12) is additional evidence that the studied samples belong to the same mineral species [10]. That this species is indeed galena is ascertained by the marked similarity (Table 3) of their powder X-ray diagrams with the corresponding diagram of galena mineral sample taken from the literature [51].

Table 3

The d-*values for the eight most intense maxima in the powder X-ray diagrams of galena from Zletovo and Sasa compared to the corresponding diagram for galena taken from literature*[a]

This work (Zletovo)	2.92_x	3.36_2	2.08_2	1.77_2	1.32_1	1.70_1	1.47_1	1.35_1
This work (Sasa)	2.93_x	3.38_3	2.08_3	1.78_2	1.32_1	1.70_1	1.48_1	1.36_1
Berry, 1972 [51]	2.97_x	3.43_8	2.10_6	1.79_4	1.33_2	1.71_2	1.48_1	1.36_1

[a] The indices in this and other similar tables denote the relative intensities of the given peaks. The index *x* is used to denote the *strongest* peak.

The above discussed results obtained by vibrational spectroscopy and powder X-ray diffraction unequivocally show that the studied four mineral samples (2 from Sasa and 2 from Zletovo) are indeed galena (PbS) minerals.

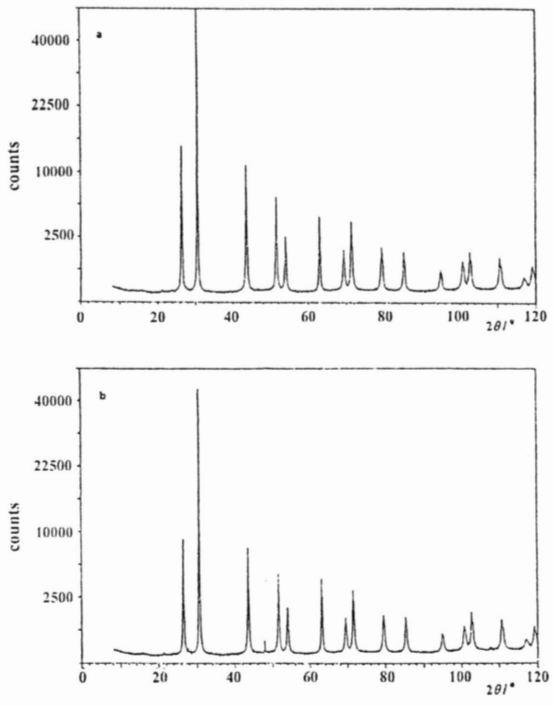

Fig. 12. The powder X-ray diagrams of galena from Sasa (a) and Zletovo (b)

Sphalerite and wurtzite

The preliminary results of the study of FT IR spectra of the (Zn,Fe)S samples from Zletovo and Toranica (Fig. 13) believed to be sphalerite have shown one broad and complex band at around 300 cm^{-1} [10]. This is not in complete agreement with the IR spectra of sphalerite and wurtzite [49] where, besides the broad band observed at about the same frequency (297 cm^{-1} for sphalerite and 299 cm^{-1} for wurtzite), an additional sub-maximum (around 334 cm^{-1}) is found for both mineral forms. The existence of this sub-maximum (around 334 cm^{-1}) was later detected in our IR spectrum of the sample from Toranica recorded by taking a small quantity (thin layer) of the studied specimen (Fig. 13c). However, the identical IR spectra of the structurally different forms of (Zn,Fe)S (sphalerite and wurtzite) [49] did not make it possible to discriminate between those two mineral forms.

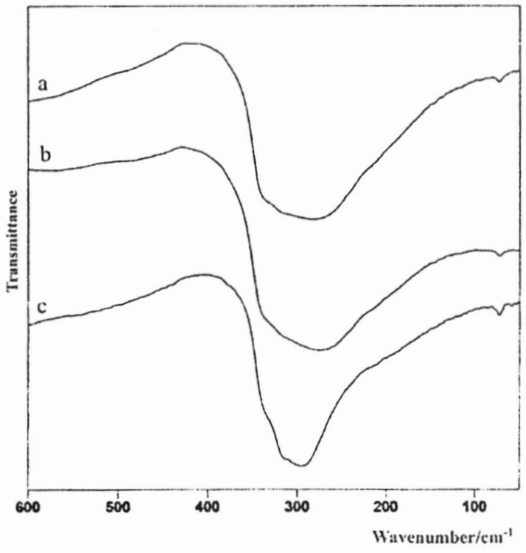

Fig. 13. The FT IR spectra of sphalerite/wurtzite from Zletovo (a), Toranica (b) (thick layer), Toranica (c) (thin layer)

Three well-defined bands with practically identical frequencies but with intensities varying from sample to sample were observed in the studied Raman spectra of the (Zn, Fe)S sample from Zletovo, Toranica and Sasa (Fig.

14) [10]. They agree well with the previously published Raman data for wurtzite [52]. Namely, the three above-mentioned bands observed in the spectra of our samples have their equivalents in the most intense bands (at 350, 327 and 297 cm^{-1}) in the published wurtzite Raman spectrum. The rest of the bands in the 500–200 cm^{-1} spectral region mentioned by Mernagh and Trudu [52] have negligible intensity. The above discussion of the Raman spectra can be regarded as an indication that the three studied (Zn,Fe)S samples belong to the wurtzite form rather than to the sphalerite one. In support of this assumption is the reported Raman spectrum of sphalerite [52], where only two intense bands were found (at 350 cm^{-1} for the LO mode and at 275 cm^{-1} for the TO mode).

The additional band observed in the studied (Zn,Fe)S samples around 214 cm^{-1} (with variable intensity on going from sample to sample) may be taken as an indication of the presence of some impurities in the studied minerals.

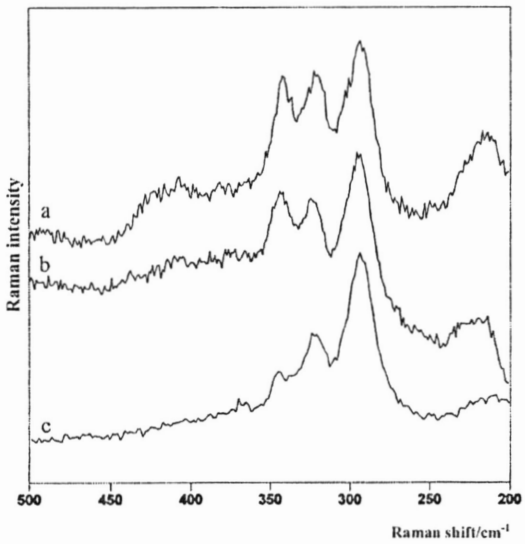

Fig. 14. The Raman spectra of sphalerite/wurtzite from Zletovo (a), Toranica (b) and Sasa (c)

For the purpose of the further identification of the studied (Zn,Fe)S mineral form, the powder X-ray diffraction diagram of the sample from Sasa was recorded (Fig. 15). The comparison of the ten most intense registered maxima in the studied powder diagram with the corresponding maxima in the diagrams of sphalerite (synthetic) and wurtzite [51] shows that eight maxima in

the synthetic sphalerite diagram (Table 4) are practically identical with the corresponding maxima in the studied diagram, whereas six most intense maxima in the diagram of the studied sample and mineral wurtzite correspond to each other. It does not confirm the previously discussed results obtained by the analysis of the Raman spectrum of the Sasa sample.

One can therefore conclude that the application of the three most frequently used instrumental techniques (IR and Raman vibrational spectroscopy and powder X-ray diffraction) for mineral identification and characterization does not necessarily and unequivocally enable discrimination between the mineral forms which often appear together and undergo transformation from one to the other form [53].

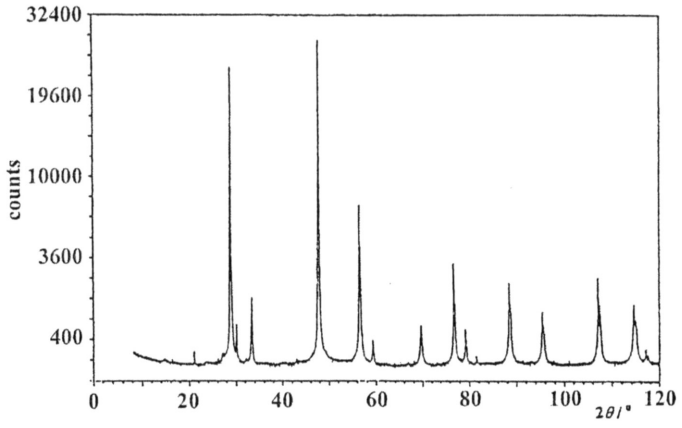

Fig. 15. The powder X-ray diagram of sphalerite/wurtzite from Sasa

Table 4

The d-*values for the ten most intense maxima in powder X-ray diagrams of sphalerite/wurtzite from Sasa compared to the corresponding values for synthetic sphalerite and mineral wurtzite taken from the literature*

This work (Sasa)	3.10_8	1.91_x	1.63_3	2.69_1	1.24_1	1.10_1	1.35_1	1.04_1	2.97_1	0.91_1
Berry, 1972 (for syn. sphalerite) [51]	3.12_x	1.91_5	1.63_3	2.71_1	1.24_1	1.10_1	1.35_1	1.04_1		
Berry, 1972 (for wurtzite) [51]	3.12_x	1.90_5	1.63_4			1.10_1			2.93_1	0.91_1

3.3. Oxide mineral samples

The Fourier transform infrared spectroscopy (FT IR) and powder X-ray diffraction (XRD) were used [19] in the process of identification of oxide minerals: hematite, Fe_2O_3; magnetite, Fe_3O_4; limonite, FeOOH; goethite, α-FeOOH; corundum, Al_2O_3; rutile, TiO_2, and chromite, $FeCr_2O_4$, collected from various localities in the Republic of Macedonia (Pehčevo, Damjan, Alšar, 'Ržanovo, Sivec, Raduša, Veselčani, Košino) [19]. In some cases the disagreements between the infrared spectra of the studied mineral types (the number of bands and their frequencies) and the corresponding literature analogues were discussed. The difficulties in their identification were solved by the analysis of their X-ray patterns which are representative for the detection of impurities in some of the studied mineral samples.

Hematite

Three hematite, Fe_2O_3, samples (two from Damjan and one from 'Ržanovo) were studied [19] in the far infrared region (Fig. 16).

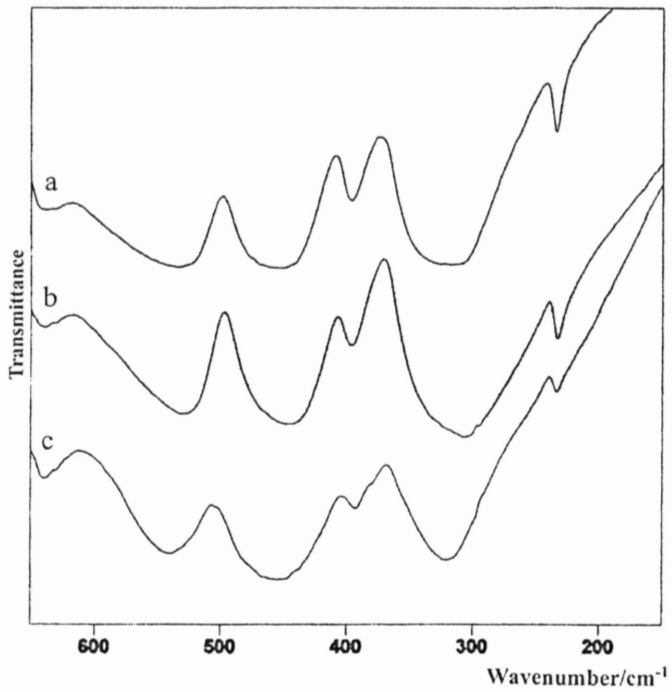

Fig. 16. The far IR spectra of hematite from Damjan (a, b) and 'Ržanovo (c)

The spectral similarity strongly indicates that the investigated samples belong to the same mineral species. The observed six bands in the spectra of the studied samples correspond, in general, to the number of the infrared bands (four to six) registered in the literature [48, 54–56] for hematite (Table 5), this being in accordance with the predictions based on the factor-group analysis [57]. It strongly suggests that the studied samples belong to mineral hematite. The observed frequency shifts of the corresponding bands (Fig. 16 and Table 5) in the studied spectra were explained as due to the influence of the particle shape and size [56].

Table 5

Band assignment and the frequencies in the IR spectra of hematite samples from Damjan and 'Ržanovo compared to corresponding literature data (in cm^{-1})

Desc.	This work			Taylor *et al.* [54], natural	Farmer[a] [48], natural	McDevitt & Baun [55], synthetic	Serna *et al.*[b] [56], synthetic	
	Damjan 1	Damjan 2	'Ržanovo					
E_u^1	641m[c]	640 m	643 m	625 sh	650 w	630 sh	–	–
E_u^2	453 s	450 s	446 s	465 s	440 s	470 s	480 s	468 s
E_u^3	315 s	320 s	307 s	335 s	–	335 s	345 s	325 s
E_u^4	233 w	233 w	233 w	–	229 w	229 w	235 w	–
A_{2u}^1	528 s	539 s	526 s	545 s	525 s	540 s	560 s	560 s
A_{2u}^2	397 w	394 w	397 w	370 sh	400 sh	380 w	370 sh	370 sh

[a] The band frequencies are approximate because numeric data are not given.

[b] First column – lath-shaped microcrystals; second column – very irregularly shaped particles.

[c] s – strong; m – medium; w – weak; sh – shoulder.

In order to confirm the indications obtained by infrared spectroscopy, the X-ray diagrams of the studied samples were obtained [19]. As seen from Tables 6 and 7, the two X-ray patterns are similar, except for the appearance of a series of peaks with higher *d*-values in the hematite diagram from 'Ržanovo (the X-ray diagrams of both Damjan samples are identical). They are related to the presence of talc as well as orthochrysotile impurities in the 'Ržanovo sample, whereas the Damjan sample contains a small quantity of quartz impurities.

Table 6

The most intense maxima in the X-ray diagram of hematite from 'Ržanovo compared to the literature data

This work			Berry & Thompson [58]	Berry (Ed.) [51]	Impurities[a]
hkl	I/I_0	d_{exp} (Å)	d_{exp} (Å)	d_{exp} (Å)	d_{exp} (Å)
	12	9.03	–		9.35_x – Talc
	25	7.99	–		?
	15	6.88	–		7.10_x – Orthochrysotile
	8	4.67	–		4.59_6 – Talc
012	29	3.62	3.68_3	3.66_3	
	10	3.51	–		3.55_7 – Orthochrysotile
	20	3.05	–		3.12_4 – Talc
104	100	2.67	2.69_{10}	2.69_x	
110	70	2.49	2.52_8	2.51_5	
	6	2.27	–		2.33_8 – Orthochrysotile
113	25	2.19	2.21_4	2.20_3	
024	36	1.83	1.843_6	1.84_4	
116	45	1.68	1.697_7	1.69_6	
122	14	1.59	1.604_3		
214	26	1.48	1.488_5	1.48_4	
300	26	1.45	1.457_5	1.45_4	
208	6	1.34	1.351_1		
10.10	13	1.31	1.313_4		
217	7	1.25	1.261_2		
312	5	1.19	1.192_2		
02.10	8	1.16	1.166_2		
134	9	1.14	1.143_4		
226	10	1.10	1.106_4		
21.10	10	1.05	1.058_5		
232	6	0.99	0.99_3		

[a] According to Berry & Thompson [58].

Table 7

The most intense maxima in the X-ray diagram of hematite from Damjan compared to literature data

This work			Berry & Thompson [58]	Berry (Ed.) [51]	Impurity[a]
Hkl	I/I_0	d_{exp} (Å)	d_{exp} (Å)	d_{exp} (Å)	d_{exp} (Å)
012	22	3.61	3.68_3	3.66_3	
	14	3.28	–		3.34_x – Quartz
104	100	2.66	2.69_{10}	2.69_x	
110	40	2.49	2.52_8	2.51_5	
	9	2.27	–		2.28_4 – Quartz
113	17	2.18	2.21_4	2.20_3	
024	27	1.83	1.843_6	1.84_4	
116	44	1.68	1.697_7	1.69_6	
122	15	1.59	1.604_3		
214	20	1.48	1.488_5	1.48_4	
300	19	1.45	1.457_5	1.45_4	
208	6	1.34	1.351_1		
10.10	19	1.30	1.313_4		
217	7	1.25	1.261_2		
312	7	1.18	1.192_2		
02.10	7	1.16	1.166_2		
134	7	1.14	1.143_4		
226	7	1.10	$1.079_{1/2}$		
21.10	10	1.05	1.058_5		
232	5	0.99	0.99_3		

[a] According to Berry and Thompson [58].

Corundum

The next studied mineral – corundum, Al_2O_3, is isomorphous with hematite [59] and thus six active IR bands are expected in its spectrum, Fig. 17. Generally, the frequencies in the spectrum studied by us [19] (Table 8) are in agreement with the literature data, [48, 50, 54–56, 60]. The differences can be mainly attributed to the shape of the particles, which provoked a remarkable influence on the frequency and the intensity of most bands due to the infrared *surface* modes. Thus, the evolution of the corundum (α–Al_2O_3) surface modes with the geometry of the particles is strongly affected for the highest-frequency modes A_{2u} and E_u, amounting from 600 to 900 cm^{-1} and from 640 to 880 cm^{-1}, respectively, and are shifted on going from the transverse to the longitudinal optical mode [56]. The observed high-frequency bands at 1087 and 969 cm^{-1} in the studied spectrum (Fig. 17, Table 8) have also previously been registered at similar frequencies [50, 54]. In addition, two very weak bands at 798 and 778 cm^{-1} are also mentioned in the literature [50, 56, 60] (Table 8). This indicates that some type of disorder in the structure is possible or that additional types of coordination of the aluminium atoms (e.g. AlO_4; AlO_3) are present in the structure [50].

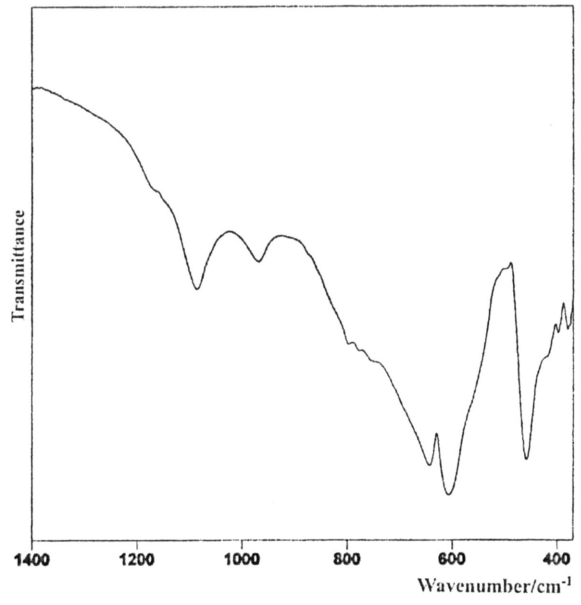

Fig. 17. The mid IR spectrum of corundum from Sivec

Table 8

Band assignment and the frequencies in the IR spectra of corundum from Sivec based on the factor group analysis and compared to corresponding literature data (in cm^{-1})

Descrip.	This work (Sivec)	Taylor *et al.* [54], nat.	Famer[a] [48], nat.	Nicodom[b] [60], nat.	Plyusnina [50], nat.	McDevitt & Baun [55], syn.	Serna *et al.*[b] [56] syn.
E_u^1	644 m[c]	640 m	630 s	642 s	620 m	–	638m 642 s
E_u^2	607 s	605 s	597 s	605 s	–	575 s	590 s 600 s
E_u^3	459 s	450 s	460 s	455 s	460 s	432 s	450 s 458 s
E_u^4	379 m	380 w	380 w	–	–	375 sh	385 w 385 m
A_{2u}^1	562 sh	–	495 w	560 sh	520 w	–	– 560 w
A_{2u}^2	398 w	–	400 sh	–	–	–	– 433 w
Not as-signed	1087 m	1085 vw		1085 s	1160 s		
	969 m	965 vw		–	1040 sh		757 w
	798 w			800 w	800 m		500 m
	778 w			780 w	680 m		

[a] The band frequencies are approximate because numeric data are not given.

[b] First column – plate-shaped particles; second column - disc and lath-shaped particles.

[c] s – strong; m – medium; w – weak; sh – shoulder.

The identity of the studied Al_2O_3 sample from Sivec was ascertained by the comparison of its powder X-ray diagram [19] with the corresponding diagram of the corundum sample taken from the literature [51] (Table 9). As seen from Table 9, the *d*-values of the eight most intense maxima in the X-ray powder diagram of the studied mineral sample are accompanied by practically the same *d*-values found in the corundum diagram. The additional peak registered at $d = 2.01$ Å is probably due to the presence of iron impurities in the form of magnetite (2.09 Å) [58].

Table 9

The most intense maxima in the X-ray diagram for corundum from Sivec compared to the literature data

This work			Berry (Ed.) [51]	Impurity[a]
hkl	I/I_0	d_{exp} (Å)	d_{exp} (Å)	d_{exp} (Å)
012	88	3.42	3.48_8	
104	100	2.52	2.55_9	
110	40	2.35	2.38_4	
113	97	2.07	2.09_x	
	11	2.01		2.09_7 – Magnetite
024	57	1.73	1.74_5	
205	8	1.62		
116	73	1.59	1.60_8	
211	6	1.54		
018	10	1.50		
124	42	1.40	1.40_3	
300	50	1.37	1.37_5	
10.10	14	1.23		
226	17	1.04		
21.10	10	1.00		

[a]According to Berry & Thompson [58].

Rutile

Four IR active modes were registered [19] in the studied far-IR spectrum of rutile sample (Fig. 18).

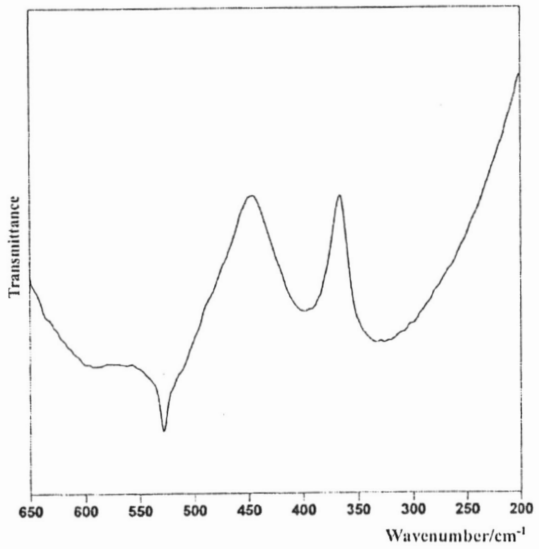

Fig. 18. The far IR spectrum of rutile from Veselčani

The IR spectrum of this mineral species is extremely sensitive to the size, shape and preparation conditions of the sample [48, 61]. This is due to the high refraction index and is predominantly expressed in the IR rather than in the corresponding Raman spectrum [48]. Therefore the number of registered bands in the literature is increased and causes broadening of the spectral region where the corresponding bands are expected [55, 62, 63] to appear (Table 10). As seen from Table 10, the observed four IR bands in the spectrum of the studied rutile sample appear in the expected broadened spectral regions. In spite of that, the identification of the minerals with a high refraction index (as is the case with the the rutile samples) should be additionally proven using more reliable methods.

X-ray powder diffraction is certainly more reliable method for the purpose of the further identification of the studied rutile sample. In Table 11 the most intense registered maxima in the studied powder diagram are listed [19] compared with the corresponding maxima in the diagrams of natural [58] and synthetic [51] rutile samples. The comparison shows that the powder X-ray patterns of natural rutile taken from literature are practically identical with those studied by us and shown in the diagram. It confirms the preliminary identification based on the investigation of the FT IR spectrum of rutile.

Table 10

Band assignment and the frequencies (in cm^{-1}) in the IR spectrum of rutile from Veselčani compared to the corresponding literature data

Description	This work (Veselčani)	Luxon & Summitt[a] [62], natural	Ocana & Serna[b] [63], natural	McDevitt & Baun [55], synthetic
E_u^1- ν_3	334 m[c]	350	365 – 345	352 w
E_u^2- ν_2	398 m	425	435 – 405	423 w
E_u^3- ν_1	528 w	610	545 – 515	608 s
A_{2u}- ν_4	600 s	680	675 – 600	695 s

[a] The intensities are not given.
[b] The range for band appearance is given because six spectra were observed. Intensity varies.
[c] s – strong; m – medium; w – weak.

Table 11

The most intense maxima in the X-ray diagram of rutile from Veselčani compared to the literature data

This work			Berry & Thompson [58]	Berry (Ed.) [51][a]
hkl	I/I_0	d_{exp} (Å)	d_{exp} (Å)	d_{exp} (Å)
110	100	3.21	3.24_{10}	3.25_x
101	32	2.46	2.49_5	2.49_5
200	8	2.23	$2.29_{1/2}$	
111	15	2.17	2.18_3	2.19_3
210	7	2.04	$2.05_{1/2}$	
211	33	1.68	1.687_7	1.69_6
220	9	1.62	1.621_3	1.62_2
002	6	1.47	1.473_1	1.46_1
130	6	1.45	1.451_1	
031	12	1.35	1.354_4	1.35_2
112	8	1.34	1.344_1	
321	5	1.18	1.169_1	
222	5	1.09	1.092_1	
141	5	1.04	$1.041_{1/2}$	

[a] Synthetic analogue.

Magnetite and chromite

Four vibrational infrared modes are expected in the spectrum of the next studied oxide mineral, magnetite, Fe_3O_4, according to factor-group analysis [57], but only two are observed by Taylor *et al.* [54] and McDevitt and Baun [55], Table 12. On the other hand, as many as ten bands are registered in the 1500–400 cm^{-1} region of the infrared spectrum of the sample considered to be magnetite [60]. Several problems occur in the process of recording the far IR spectra of the studied [19] magnetite samples from Damjan and Košino (Fig. 19) due to the powdered the sample particle size and the weakness of the bands in the spectrum [48, 55]. Therefore, additional powdering of the sample was undertaken in order to record the mid-infrared spectra of magnetite using KBr pressed discs and to reduce the scattering, Fig. 19. Consequently, the maximum of the most intensive band in the far IR of magnetite from Damjan at 553 cm^{-1} is blue shifted by 6 cm^{-1} in the mid IR spectrum. The same band in the mid-IR spectrum of the magnetite sample from Košino is shifted by 20 cm^{-1}, being much closer to the frequency found in the literature [54, 55]. Furthermore, the band in the studied mid-IR spectrum of the Damjan sample at 396 cm^{-1} agrees well with the corresponding one registered in the literature [54, 55], whereas the band at 455 cm^{-1} is not registered in the mentioned sources (see Table 12). Additional bands in the mid-infrared spectra of the Damjan sample (at 386 cm^{-1}) and the Košino sample (at 389 and 384 cm^{-1}) were observed, as well. In this context, it can be mentioned that our IR spectra of the studied samples are in better agreement with the theoretically expected four bands [57] than the published data [54, 55] where only two bands are observed.

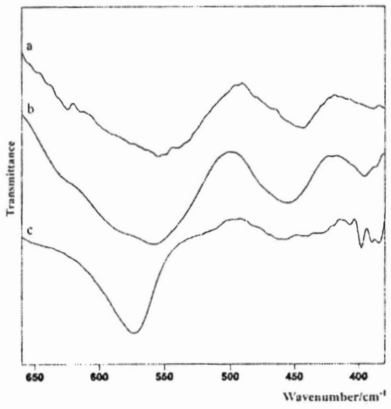

Fig. 19. The far (a) and mid (b) IR spectra of magnetite from Damjan and mid IR spectrum of magnetite from Košino (c)

Table 12

The frequencies and intensities of the bands in the far and mid-IR spectra of magnetite from Damjan and Košino compared to the literature data (in cm^{-1})

Magnetite (Damjan) – far IR	553 sb[a]	442 mb	388 wb	–
Magnetite (Damjan) – mid IR	559 sb	455 mb	396 mb	386 vw
Magnetite (Košino) – mid IR	573 sb	459 mb	398 w	389 w, 384 w
Taylor *et al.* [54] – natural	570 sb	–	385 mb	–
McDavitt & Baun [55] – synthetic	570 sb	–	385 mb	–

[a] s – strong; m – medium; w – weak; b – broad; v – very.

In order to confirm the results obtained by the IR study and to identify the studied minerals, the X-ray patterns of the two magnetite mineral samples from Košino and Damjan were studied [19] (Tables 13, 14). In general, the diagram of the studied magnetite sample from Damjan corresponds to the literature data, but additional peaks are registered due to the presence of higher quantities of quartz and dolomite impurities (Table 13). On the other hand, only two maxima are observed in the diagram of magnetite from Košino with a much lower quartz content (Table 14).

As in the case of magnetite, four vibrational infrared modes are expected [57] in the spectrum of isomorphous chromite, $FeCr_2O_4$ (Fig. 20).

In addition to expected four IR active modes registered in the region from 690 to 440 cm^{-1} (Fig. 20), five less intensive bands appeared [19] in its spectrum (Table 15). Undoubtedly, two of them (those at 3439 and 1630 cm^{-1} at room temperature) are due to the presence of surface adsorbed water molecules, whereas the highest frequency band at 3690 cm^{-1} corresponds to the $\nu(H_2O)$ mode of the free water molecule. The remaining two bands (at 1084 and 958 cm^{-1}) may be due to the presence of some silicate impurities [19]. Table 15 shows that, apart from the above mentioned two bands due to the adsorbed water molecules, the spectrum of the studied chromite sample is in a complete agreement with the IR spectrum of chromite from the literature [60], including the two bands around 1080 and 955 cm^{-1} (Table 15).

Table 13

The most intense maxima in the X-ray diagram of magnetite from Damjan compared to the literature data

	This work		Berry & Thompson [58]	Berry (Ed.) [51]	Impurity[a]
hkl	I/I_0	d_{exp} (Å)	d_{exp} (Å)	d_{exp} (Å)	d_{exp} (Å)
111	11	4.74	4.84_3		
	11	4.10	–		4.25_6 – Quartz
	10	3.63	–		3.69_2 – Dolomite
	11	3.30	–		3.34_x – Quartz
022	16	2.94	2.96_6	2.97_7	
	35	2.92	–		2.88_x – Dolomite
	23	2.67	–		2.67_3 – Dolomite
113	100	2.50	2.53_{10}	2.53_x	
	10	2.45	–		2.46_3 – Quartz
222	13	2.40	2.42_1		
	10	2.19	–		2.13_3 – Quartz
004	23	2.08	2.09_7	2.10_7	
	10	1.83	–		1.817_5 – Quartz
224	14	1.70	1.712_4	1.71_6	
	13	1.68	–		1.672_3 – Quartz
115	25	1.61	1.611_8	1.61_9	
044	35	1.47	1.481_9	1.48_9	
135	10	1.44	$1.416_{1/2}$		
026	7	1.32	1.327_2		
335	10	1.27	1.280_4		
137	8	1.09	1.094_8	1.09_6	
228	7	0.97	0.990_4		

[a] According to Berry & Thompson [58].

Table 14

The most intense maxima in the X-ray diagram of magnetite from Košino compared to the literature data

	This work		Berry & Thompson [58]	Berry (Ed.) [51]	Impurity[a]
hkl	I/I_0	d_{exp} (Å)	d_{exp} (Å)	d_{exp} (Å)	d_{exp} (Å)
111	12	4.74	4.84_3		
	11	3.29	–		3.34_x – Quartz
022	26	2.93	2.96_6	2.97_7	
113	100	2.52	2.53_{10}	2.53_x	
	22	2.49	–		2.46_3 – Quartz
222	10	2.40	2.42_1		
004	39	2.08	2.09_7	2.10_7	
224	10	1.70	1.712_4	1.71_6	
115	29	1.61	1.611_8	1.61_9	
044	28	1.48	1.481_9	1.48_9	
026	6	1.32	1.327_2		
335	8	1.28	1.280_4		
226	6	1.26	1.264_1		
246	6	1.12	1.122_4		
137	13	1.09	1.094_8	1.09_6	
008	6	1.05	1.050_5		
228	9	0.97	0.990_4		

[a] According to Berry & Thompson [58].

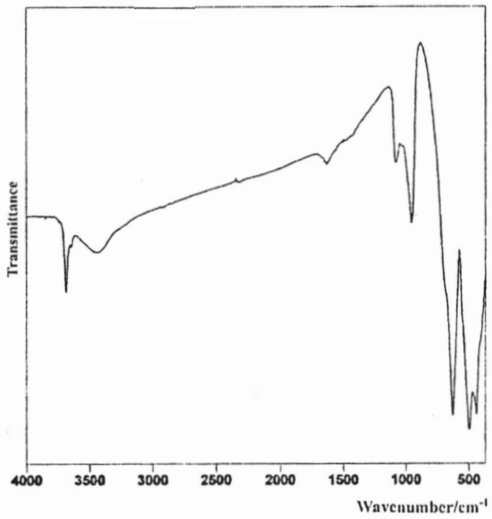

Fig. 20. The mid IR spectrum of chromite from Raduša

Table 15

The frequencies and intensities of the fundamental vibrations in the IR spectrum of chromite from Raduša compared to the corresponding literature data (in cm^{-1})

This work (Raduša)	3690 w	3439 w	1630 w	1084 w	958 m	690 sh	630 s	500 s	441s
Nicodom [60]	3680 m	–	–	1080 m	955 m	690 sh	635 s	502 s	450 sh

Since the identification of this mineral based on the study of its IR spectrum was accompanied by some difficulties, further investigation of the chromite sample from Raduša by powder X-ray diffraction was performed [19] (Table 16). The comparison with the literature data [51, 58] shows that all expected maxima are found in the studied diagram. Exceptions are the peaks at *d*-values 2.37, 1.40 and 0.96 Å, which are probably due to the presence of silicate impurities in the studied sample. It should be mentioned that in the case of the isomorphous chromite and magnetite, solid solutions may also exist in the studied sample.

Table 16

The most intense maxima in the X-ray diagram of chromite from Raduša compared to the literature data

This work			Berry & Thompson [58]	Berry (Ed.) [51]
hkl	I/I_0	d_{exp} (Å)	d_{exp} (Å)	d_{exp} (Å)
111	45	4.69	4.80_4	4.82_5
022	19	2.90	2.95_2	2.95_6
113	100	2.48	2.51_{10}	2.52_x
	12	2.37[a]	–	
004	26	2.06	2.08_5	2.07_7
224	9	1.69	$1.704_{1/2}$	
115	53	1.59	1.602_6	1.60_9
044	24	1.46	1.473_8	1.46_9
	5	1.40[a]	–	
335	19	1.26	1.271_1	1.10_6
226	6	1.25	$1.254_{1/2}$	
444	30	1.19	1.201_1	
117	6	1.16	$1.166_{1/2}$	
246	6	1.11	1.112_1	1.10_6
355	11	1.08	1.084_9	
008	6	1.04	1.041_4	
	20	0.96[a]	–	

[a] Impurity.

Limonite

One of the studied oxide mineral samples is limonite, FeOOH [19]. Generally, the term *limonite* is used for mixtures of various iron oxide and hydroxide minerals, the most common among them being goethite, α-FeOOH, and lepidocrocite, γ-FeOOH. The IR spectra of goethite and lepidocrocite are discussed by various authors [57, 60, 64–68] but disagreements among the literature data for goethite and lepidocrocite mineral forms (especially in the region of the OH stretchings) are found (Table 17). The detailed analysis of the IR spectral features (Fig. 21) of the studied limonite mineral sample from Pehčevo in the region of the OH modes (Table 17) indicates the presence of a mixture of the two mineral forms (goethite and lepidocrocite).

Table 17

Summarized literature data for the infrared spectra of goethite and lepidocrocite compared with our data for the studied goethite and limonite samples

Goethite				This work		Lepidocrocite		Quartz
Plyusnina [50]	Nicodom [60]	Ryskin[a] [67]	White & Roy [68]	Alšar	Pehčevo	White & Roy [68]	Ryskin[a] [67]	Sasa
					3510			
3420 $\nu(H_2O)$	3460			3419	3483			
					3388		3390 ν(OH)	
3330 $\nu(H_2O)$								
3200 ν(Fe–O–H)								
	3100	3095 ν(OH)		3117	3141			
			2985 ν(OH)					
						2857 ν(OH)		
	1740				1791			
1640 δ(H–O–H)	1640			1637	1630			
	1460				1434			
	1425							
					1166	1145 ?	1161 δ(OH)	1183
				1096	1090			1093
				1017	1027	1013 δ(OH)		
900 δ(Fe–O–H)	900	890 δ(OH)		893	901			
			882 δ(OH)		877	881[b]		
800 δ(Fe–O–H)	800	797 γ(OH)	793 ν(Fe–O)	799	798			799
	725				779	738 ν(Fe–O)	753 γ(OH)	779
665 ?(Fe–O)	682			667	683			694
			599 ν(Fe–O)		600			
	570			570	543			516
453 ν(Fe–O...Fe)	460		450 ?	472	470	465 ?		460
400 ν(Fe–O...Fe)	425			407	397			396
365 ν(Fe–O...Fe)								
270 δ(Fe–O–Fe)								

[a] Only the bands concerning the OH vibrations are discussed.
[b] Due to the presence of 10 % of goethite in lepidocrocite.

The study of the IR spectrum of the goethite sample collected from Alšar showed a drastic intensity decrease in the two strong bands at 1085 and 1037 cm^{-1} found in the spectrum of limonite (Fig. 21). The rest of the bands in

the IR spectrum do not change (have almost equal intensities and frequencies), this being in a good agreement with literature data (Table 17). Contrary to the above-mentioned indication about the existence of a mixture of goethite and lepidocrocite, it is evident that the studied limoniteple from Pehčevo is, in fact, a mixture of goethite and some other mineral, and not lepidocrocite [19].

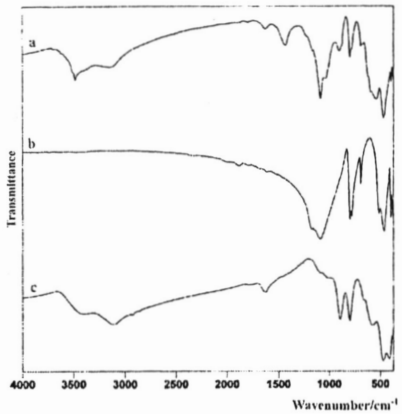

Fig. 21. The mid IR spectra of limonite from Pehčevo (a), quartz (b) and goethite from Alšar (c)

The performed chemical analysis [19] showed that the limonite sample contained 23.65 % silicon, whereas the content of Si in the goethite sample was significantly lower. In order to identify the nature of the silicate impurity present in the limonite sample from Pehčevo, the IR spectra of the limonite, goethite and quartz were compared, Fig. 21. The comparison showed that the bands at 1085, 1037, 779, 683 and 470 cm^{-1} in the spectrum of the limonite sample from Pehčevo arise from the quartz impurity, so that quartz is undoubtedly the dominant impurity in the studied limonite [19].

In order to confirm the above assumption, the X-ray patterns of the studied limonite, goethite and quartz samples were recorded. The summarized results of the powdered X-ray analysis of limonite compared with the corresponding literature data for goethite and quartz are shown in Table 18. There is no doubt that a high content of quartz impurity is present in the studied limonite sample (see maxima at *d*-values 2.46, 2.22 and 1.54 Å). On the other hand, the goethite form of the studied sample is manifested by the powder X-ray peaks registered at *d*-values 2.68, 2.56, 2.48, 2.44, 2.18, 1.71, 1.69, 1.56, 1.51, 1.48 and 1.37 Å. The remaining maxima are common to both minerals (goethite and quartz) and appear at very similar *d*-values (see Table 18).

Table 18

The most intense maxima in the X-ray diagram of limonite from Pehčevo and quartz from Sasa compared to the literature data

This work			Berry & Thompson[a] [58]	Makreski & Jovanovski[b], unpublished	Berry & Thompson[b] [58]
hkl	I/I_0	d_{exp} (Å)	d_{exp} (Å)	d_{exp} (Å)	d_{exp} (Å)
110	53	4.19	4.21_{10}	4.08_3	4.25_6
	13	3.63	–	–	–
120	100	3.31	3.37_2	3.28_{10}	3.34_{10}
	11	2.95	–	–	–
130	33	2.68	2.69_8	–	–
021	9	2.56	2.57_2	–	–
040	13	2.48	2.48_2	–	–
	11	2.46	–	2.43_1	2.46_3
111	20	2.44	2.44_7	–	–
121	13	2.26	2.25_2	–	2.28_3
	11	2.22	–	2.21_1	2.23_2
140	10	2.18	2.18_4	–	–
220	11	2.11	$2.09_{1/2}$	$2.06_{1/2}$	2.13_3
131	7	1.97	2.00_1	$1.97_{1/2}$	1.997_2
211	16	1.81	1.803_2	$1.812_{1/2}$	1.817_5
221	9	1.71	1.719_5	–	–
240	17	1.69	1.689_2	–	–
060	9	1.66	1.660_1	$1.669_{1/2}$	1.672_3
151	6	1.56	1.563_3	–	–
	13	1.54	–	1.540_2	1.542_4
250	6	1.51	1.507_2	–	–
061	12	1.48	$1.456_{1/2}$	–	–
022	16	1.45	1.452_2	$1.449_{1/2}$	1.455_2
330	10	1.38	1.392_1	–	1.379_6
170	11	1.37	1.360_1	–	–
321	7	1.31	1.318_2	1.343_1	–
042	7	1.28	$1.293_{1/2}$	–	1.29_2

[a] For goethite.
[b] For quartz.

The powder X-ray pattern of goethite from Alšar showed a much higher degree of similarity with the corresponding literature data (Table 19). A single exception is the intense peak at $d = 3.31$ Å due to the quartz impurities in the sample.

Table 19

The maxima in the X-ray diagram of goethite from Alšar compared to the literature data

This work			Berry & Thompson [58]	Berry (Ed.) [51]	Impurity[a]
hkl	I/I_o	d_{exp} (Å)	d_{exp} (Å)	d_{exp} (Å)	d_{exp} (Å)
020	20	5.03	5.02_2	4.98_1	
110	100	4.12	4.21_{10}	4.18_x	
120	15	3.39	3.37_2		
	79	3.31	–		3.34_x – Quartz
130	45	2.67	2.69_8	2.69_3	
021	33	2.56	2.57_2		
040	28	2.54	2.48_2	2.49_2	
111	79	2.43	2.44_7	2.45_3	
121	28	2.23	2.25_2		
140	26	2.18	2.18_4	2.19_2	
220	11	2.12	$2.09_{1/2}$		
131	11	2.00	2.00_1		
041	10	1.93	1.92_1		
211	19	1.81	1.803_2		
141	12	1.78	$1.774_{1/2}$		
221	39	1.73	1.719_5	1.72_2	
240	22	1.69	1.689_2		
060	13	1.66	1.66_1		
231	14	1.60	1.602_2		
151	36	1.56	1.563_3	1.56_2	
250	21	1.50	1.507_2		
022	17	1.45	1.452_2		
112	12	1.42	$1.420_{1/2}$		
330	11	1.39	1.392_1		
170	13	1.37	1.36_1		
251	10	1.35	1.347_1		
321	14	1.31	1.318_2		
042	8	1.28	$1.293_{1/2}$		
202	9	1.26	1.263_1		
171	9	1.24	1.239_1		
341	9	1.20	1.197_1		
081	10	1.15	1.151_1		
410	9	1.14	1.141_1		
351	10	1.12	1.125_1		
190	7	1.08	$1.077_{1/2}$		
361	9	1.06	1.056_1		
431	11	1.02	1.024_2		
191	11	1.01	1.014_2		
0.10.0	7	0.98	0.996_1		

[a] According to Berry and Thompson [58].

The analysis of the oxide minerals shows that both far and mid IR spectra are useful and can serve as a powerful qualitative tool for the identification and characterization of the minerals. However, in acquiring good-quality spectra, the problems concerning the particle size and form as well as the sample powdering and preparation should not be underestimated. Significant disagreement between various infrared literature data for the same mineral (especially for limonite) may cause additional difficulties in the identification of the studied minerals. On the other hand, the powder X-ray diffraction technique gives an unambiguous opportunity for mineral identification, simultaneously enabling a rapid check on their purity. Although both techniques are complementary rather than competitive, the study of oxide minerals proves that the powder X-ray diffraction is more sensitive to mineral impurities determination compared to the FT IR spectroscopy [19].

Nesosilicate mineral samples

In order to be identified and characterized, the vibrational (infrared and Raman) spectra and powder X-ray diffraction patterns of seven common nesosilicate minerals from the Republic of Macedonia were also studied. These were almandine, $Fe_3Al_2(SiO_4)_3$; spessartine, $Mn_3Al_2(SiO_4)_3$; zircon, $ZrSiO_4$; titanite, $CaTiOSiO_4$; olivine, $(Mg,Fe)_2SiO_4$; kyanite, Al_2OSiO_4 and staurolite, $Fe_2Al_9O_6(SiO_4)_4(OH)_2$ [17, 21, 69].

Several studies have been undertaken to study IR spectra of almandine [60, 70–73], spessartine [60, 71–73], zircon [60, 74–76], titanite [60], olivine [60, 71, 77, 78], kyanite [60, 79, 80] and staurolite [60, 81]. Also, Raman spectra of almandine [72, 73, 82–85], spessartine [73, 82–84], zircon [82, 85], titanite [82, 86], olivine [82, 87] and kyanite [88] were additionally used for mineral characterization. The Raman spectrum of staurolite, to the best of our knowledge, has not been published in the literature.

The main structural feature of the nesosilicate minerals is that the tetrahedral SiO_4^{4-} anions are not bonded to the other tetrahedra, the net negative charge of the isolated silicon-containing tetrahedral ion being balanced cations such as Mg^{2+}, Fe^{2+}, Al^{3+} etc [45]. Almandine, $Fe_3Al_2(SiO_4)_3$, and spessartine, $Mn_3Al_2(SiO_4)_3$, are isomorphous minerals, whereas olivine, $(Mg,Fe)_2SiO_4$, is, in fact, a solid solution with varying content of isomorphous forsterite, Mg_2SiO_4, and fayalite, Fe_2SiO_4 (the end members of this series of solid solutions). The remaining four minerals (zircon, titanite, kyanite and staurolite) are structurally different. The cation (Al^{3+}, Mg^{2+}, Fe^{2+}, Zr^{4+}) coordination spheres in the struc-

tures of almandine, spessartine, olivine and zircon consist of oxygens belonging to the silicon-containing tetrahedra, whereas the coordination spheres of the cations (Al^{3+}, Fe^{2+}, Ca^{2+}, Ti^{4+}) in the kyanite, staurolite and titanite structures, in addition to the SiO_4 oxygens, are also coordinated by O and/or OH that are not part of the silicon-containing tetrahedra.

Almandine and spessartine

In order to relate the vibrational and the crystallographic characteristics of the isomorphous minerals almandine (from Pelagon) and spessartine (from Lojane), their powder IR absorption spectra (Fig. 22) as well as their Raman spectra (Fig. 23) were studied. As seen from Fig. 22, the IR spectra of almandine and spessartine are practically identical and, in general, in accordance with the corresponding literature data (Tables 20 and 21 and the references therein). Two well-defined spectral regions are observed for both spectra [21]. The bands in the first region (1000–800 cm^{-1}) arise from the high-energy ν_3 modes of the main SiO_4 vibrational units, whereas the second well-developed region (700–400 cm^{-1}) consists of bands due to ν_4 and ν_2 modes of the SiO_4 tetrahedra (Fig. 22 and Tables 20 and 21) [73]. It should be pointed out that, compared to the corresponding modes in the spectrum of almandine, a decreasing trend was registered for the ν_3 frequency modes and for the bands in the 650–500 cm^{-1} region of the spessartine spectrum. This means that the vibrational frequencies of the almandine with a smaller unit cell volume (1533.2 $Å^3$) are, in general, higher than those of spessartine whose unit cell volume is larger (1565.7 $Å^3$) [21].

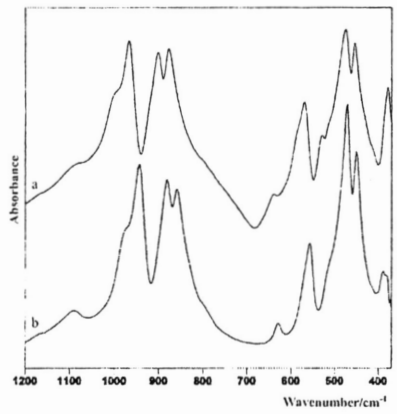

Fig. 22. Infrared spectra of almandine from Pelagon (a) and spessartine from Lojane (b)

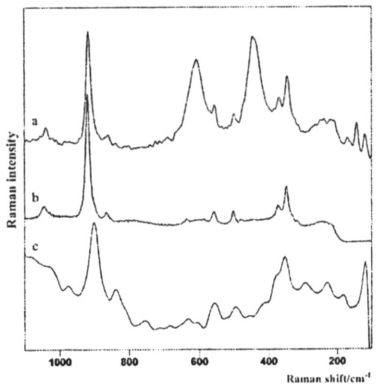

Fig. 23. Micro-Raman spectra of almandine from Pelagon (a, b) excited with the 1064 and 514 nm lines, respectively, and micro-Raman spectrum of spessartine from Lojane (c) excited using the 1064 nm line

Table 20

Frequencies and intensities of the bands in the powder IR spectrum of almandine from Pelagon compared with the corresponding literature data (in cm^{-1})

This work	Nicodom[a] [60]	Moore *et al.*[b] [72]	Moenke[a] [71]	Hofmeister & Chopelas[c-e] [73]		Bofa *et al.*[a,f-g] [70]	Assignment[h]
				LO	TO		
379 m		376		396	376	378 s	SiO_4 rotations
455 s	454 m	448	455 m	518	448	442 m	ν_2
476 s	475 m	469	480 m	461	468	465 vs	Al translations
530 w	530 vw	526	527 s	534	525	525 w	ν_4
571 s	568 s	571	–	597	561	570 vs	ν_4
640 w	640 vw	635	638 m	638	634	635 w	ν_4
877 s	887 s	870	872 s	882	889	875 s	ν_3
901 s	899 s	897	902 s	923	865	900 s	ν_3
967 vs	965 s	960	970 vs	1038	952	970 vs	ν_3
998 sh	993 sh	991				995 sh	
–	1043 sh	–				–	
1085 sh	1096 sh	–				1085 sh	

[a] Wavenumbers are approximate because explicit numerical data are not given.
[b] Additional bands are found at 116, 137, 156, 192, 237, 317 and 338 cm^{-1}.
[c] Intensities are not given.
[d] IR reflectance spectrum.
[e] Additional bands are found at 115, 147, 160, 205, 246, 322, 347, 422 cm^{-1} (LO) and 111, 137, 158, 196, 236, 318, 345, 412 cm^{-1} (TO).
[f] Synthetic sample.
[g] Additional bands are found at 116, 137, 158, 200, 237, 316 and 342 cm^{-1}.
[h] According to Hofmeister & Chopelas [73].

Table 21

Frequencies and intensities of the bands in the powder IR spectrum of spessartine from Lojane compared with the corresponding literature data (in cm^{-1})

This work	Nicodom[a] [60]	Moore *et al.*[b] [72]	Moenke[a] [71]	Hofmeister & Chopelas[c-e] [73]		Assignment[f]
				LO	TO	
384 w		379		383	380	SiO_4 rotations
451 m	449 m	447	452 s	531	445	ν_2
471 s	470 s	470	472 s	458	461	Al translations
511 sh	513 sh	495	–	517	520	ν_4
558 s	560 s	565	562 s	593	558	ν_4
630 w	630 m	631	632 m	638	630	ν_4
859 s	860 s	861	870 s	912	861	ν_3
881 s	883 s	895	892 s	871	884	ν_3
944 s	944 s	949	955 vs	1030	946	ν_3
976 sh	978 sh	976	–			
1089 w	1088 w	–	–			

[a] Wavenumbers are approximate because explicit numerical data are not given.
[b] Additional bands are found at 113, 140, 165, 203, 242, 308 and 341 cm^{-1}.
[c] Intensities are not given.
[d] IR reflectance spectrum.
[e] Additional bands are found at 115, 150, 168, 212, 249, 320, 352, 414 cm^{-1} (LO) and 111, 140, 167, 203, 246, 316, 350 cm^{-1} (TO).
[f] According to Hofmeister & Chopelas [73].

As seen from Fig. 23, two Raman spectra of almandine on different instruments and with different excitation lines (1064 and 514 nm) are recorded, whereas the attempt to record the spessartine spectrum with the 514 nm line failed [21]. The Raman spectra of the same almandine specimen recorded with various excitation lines are, to some extent, similar, but show some significant differences (Table 22) suggesting that one should be careful during their use for identification purposes as well as for spectra–structure correlations. In fact, all bands observed in the Raman spectrum taken with the 514 nm excitation line are present in the spectrum obtained with the 1064 nm excitation line, where two additional strong bands at 446 and 607 cm^{-1} were registered. Since the former Raman spectrum (that excited with the 514 nm line) shows a closer similarity with the corresponding spectrum of the isomorphous spessartine analogue (Table 23), it is more likely that some structural changes appear during the recording of the almandine Raman spectrum excited with the 1064 nm line.

Table 22

Frequencies of the bands in the powder Raman spectrum of almandine from Pelagon compared with the corresponding literature data (in cm^{-1})

This work[a,b]	This work[c]	Calligaro *et al.*[d] [85]	Moore *et al.*[d,e] [72]	Kolesov & Geiger[d] [84]	Hofmeister & Chopelas[d] [73]	Griffith [82]	Assignment[f]
147 m		–	–	167	163		Fe translations
170 w		168	–	170	166		Fe translations
208 w		–	–	–	198		SiO_4 translations
218 w	–	–	–	216	212	–	Fe translations
238 w	240 w	–	266	256	239	–	SiO_4 translations
299 vw	–	–	–	–	293	–	SiO_4 translations
–	318 vw	–	–	314	312	–	SiO_4 rotations
–	–	–	–	323	326	–	SiO_4 translations
343 m	349 m	347	307	342	347	340	SiO_4 rotations
–	–	–	–	–	355	–	SiO_4 rotations
371 w	372 w	370	400	370	368	–	SiO_4 rotations
446? vs	–	–	–	–	421	–	ν_2
–	481 vw	–	468	475	474	–	ν_2
500 w	502 m	501	-	500	498	–	ν_4
523 vw	–	–	517	–	521	–	ν_2
555 w	559 m	557	562	556	553	–	ν_2
570 vw	586 vw	–	–	581	576	–	ν_4
607? vs	–	–	611	596	593	–	ν_4
–	636 w	625	644	630	628	–	ν_4
690 w	687 vw	683	695	–	–	–	–
–	–	–	745	–	–	–	–
801 w	–	–	806	–	–	–	–
861 w	865 w	862	843	863	862	870	ν_3
–	–	–	–	897	892	900	ν_3
917 vs	921 vs	917	890	916	910	–	ν_1
–	–	–	–	930	920	917	ν_3
1041 m	1044 m	1042		1038	1032	960	ν_3

[a] Excitation with 1064 nm.
[b] Additional very weak bands appear at 118, 142, 250, 263, 271, 286, 384, 512, 535 and 14 more in 700–1050 cm^{-1}.
[c] Excitation with the 514 nm line.
[d] Single crystal.
[e] The specimen contains 23 % pyrope, $Mg_3Al_2(SiO_4)_3$.
[f] According to Hofmeister & Chopelas [73].

Table 23

Frequencies of the bands in the powder Raman spectrum of spessartine from Lojane compared with the corresponding literature data (in cm^{-1})

This work[a,b]	Moore *et al.*[c,d] [72]	Kolesov & Geiger[c] [84]	Hofmeister & Chopelas[c] [73]	Griffith [82]	Assignment[e]
–	–	162	162		Mn translations
183 w	–	175	173		Mn translations
–	–	196	194		SiO_4 translations
228 w	–	221	220		Mn translations
–	–	269	229	–	SiO_4 translations
293 w	–	302	300	–	SiO_4 translations
–	–	321	318	–	SiO_4 translations
–	–	–	347	–	SiO_4 translations
354 m	–	350	350	360	SiO_4 rotations
377 sh	–	372	372	–	SiO_4 rotations
413 vw	–	–	410	456	ν_2
454 vw	–	475	472	470	ν_2
496 m	503	500	499	–	ν_4
–	–	522	521	–	ν_2
557 m	–	552	550	560	ν_2
607 vw	–	–	592	–	ν_4
632 vw	617	630	628	–	ν_4
838 w	–	849	849	–	ν_3
–	–	879	878	880	ν_3
–	–	–	892	–	ν_1
901 s	896	905	905	–	ν_1
–	–	–	913	916	ν_3
976 vw	–	–	–	–	ν_3
1025 sh	–	1029	1027	–	ν_3

[a] Excitation with the 1064 nm.
[b] Additional very weak bands appear at 684, 712 and 754 cm^{-1}.
[c] Single crystal.
[d] The specimen contains 22 % almandine, $Fe_3Al_2(SiO_4)_3$.
[e] According to Hofmeister & Chopelas [73].

It should be pointed out here that the predicted number of bands in the Raman spectra of both garnet minerals (almandine and spessartine) by the factor-group analysis is 25 [72], which makes, in general, the Raman spectra more complex then the corresponding IR spectra. In spite of that, in general, the Raman spectra of the two garnet minerals agree well with the corresponding literature data (Tables 22 and 23 and references therein), confirming that the studied mineral samples indeed belong to almandine and spessartine. The closer examination of the frequencies of the stretching and the bending vibrations in the Raman and IR spectra, respectively, shows that they are, in general, consistent (e.g. IR–Raman 'doublets' appear) (Tables 20–23).

The identification of the studied almandine and spessartine mineral samples was confirmed by the study of their powder X-ray diffraction patterns (Fig. 24 and Tables 24 and 25). Namely, as seen from Tables 23 and 24, the X-ray diagrams of the studied almandine and spessartine are in a complete agreement with the corresponding literature data [89]. In spite of the practical identity between the X-ray diagrams of the two studied garnet mineral samples (Fig. 24), there are two weak peaks in the almandine diagram (d-values of 3.3313 and 0.9342 Å), which are absent in the diagram of the spessartine analogue. They enable the discrimination between these two isomorphous garnet minerals using powder X-ray diffraction.

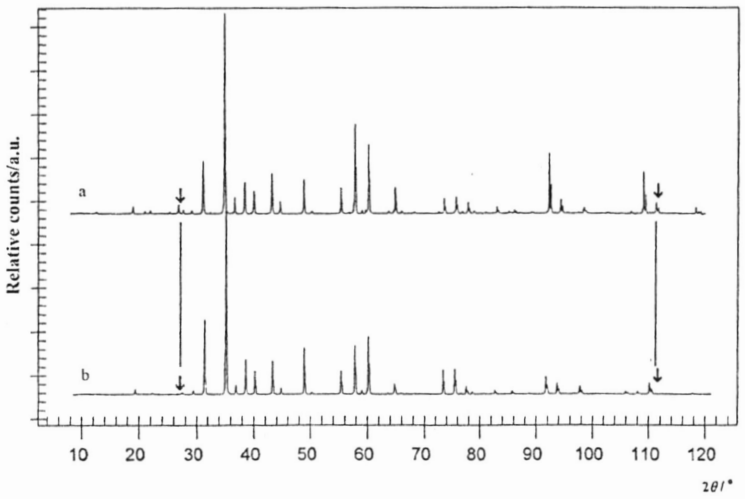

Fig. 24. Powder X-ray patterns of almandine from Pelagon (a) and spessartine from Lojane (b). The peaks present in almandine which are absent in the spessartine diagram are denoted by arrows

Table 24

The maxima in the X-ray diagram of almandine from Pelagon compared to the literature data

This work			ICDD, PDF-4 /Minerals [89]	This work			ICDD, PDF-4 /Minerals [89]
hkl	I/I_0	d_{exp} (Å)	d_{exp} (Å)	*hkl*	I/I_0	d_{exp} (Å)	d_{exp} (Å)
210	7	4.7112	-	741	4	1.4205	1.4200
200	5	4.0800	-	653	4	1.3793	1.3800
310	4	3.6493	-	840	17	1.2902	1.2900
222	8	3.3313	3.3300	842	23	1.2592	1.2600
321	4	3.0842	-	761	4	1.2444	1.2400
400	28	2.8850	2.8800	664	9	1.2302	1.2300
330	4	2.7200	2.7200	851	5	1.2164	1.2200
420	100	2.5804	2.5800	932	4	1.1902	-
332	12	2.4603	2.4600	941	6	1.1657	1.1700
422	18	2.3556	2.3500	10.11	4	1.1426	-
431	14	2.2632	2.2600	10.20	5	1.1316	1.1300
521	22	2.1069	2.1100	10.40	53	1.0715	1.0700
440	10	2.0400	2.0400	10.42	11	1.0535	1.0500
611	22	1.8720	1.8700	880	6	1.0200	1.0200
620	4	1.8246	1.8200	12.00	4	0.9617	0.9600
444	16	1.6657	1.6700	12.20	25	0.9550	0.9500
543	4	1.6320	1.6300	10.71	12	0.9422	0.9400
640	58	1.6003	1.6000	10.64	9	0.9360	0.9379
721	9	1.5704	1.5700	12.31	8	0.9342	0.9318
642	38	1.5421	1.5400	900	4	0.9067	0.8975
800	18	1.1425	1.4400				

Table 25

The maxima in the X-ray diagram of spessartine from Lojane compared to the literature data

This work			ICDD, PDF-4 /Minerals [89]	This work			ICDD, PDF-4 /Minerals [89]
hkl	I/I_0	d_{exp} (Å)	d_{exp} (Å)	*hkl*	I/I_0	d_{exp} (Å)	d_{exp} (Å)
211	5	4.7357	–	642	30	1.5501	1.5500
222	4	3.3486	–	651	3	1.4732	–
321	5	3.1002	–	800	8	1.4500	1.4500
400	38	2.9000	2.9000	741	3	1.4279	–
420	100	2.5938	2.6000	840	18	1.2969	1.3000
332	7	2.4731	2.4800	842	25	1.2657	1.2700
422	19	2.3678	2.3700	664	7	1.2366	1.2400
431	15	2.2749	2.2800	930	4	1.2227	1.2300
521	20	2.1179	2.1200	941	8	1.1718	1.1700
440	6	2.0506	2.0500	10.20	4	1.1375	1.1400
611	25	1.8817	1.8900	10.40	20	1.0864	1.0800
620	4	1.8341	–	10.42	12	1.0589	1.0600
444	15	1.6743	1.6800	10.51	11	1.0334	1.0300
543	3	1.6405	1.6400	965	8	0.9734	0.9700
640	27	1.6086	1.6100	981	8	0.9600	0.9600
721	5	1.5786	1.5800	12.22	11	0.9409	0.9400

Zircon

The band assignments in the IR spectrum (Fig. 25) of the next studied zircon sample from Kozjak [21] was again based on the concept of group frequencies of the SiO_4 tetrahedra as the main vibrational units in the structure as well as on the comparison with the corresponding IR data published by various authors [60, 74–76], (Table 26). As seen from Table 26, the IR spectrum of the studied sample (supposedly, zircon) is in complete agreement with the literature data and this is taken as a first indication that the studied mineral is indeed zircon.

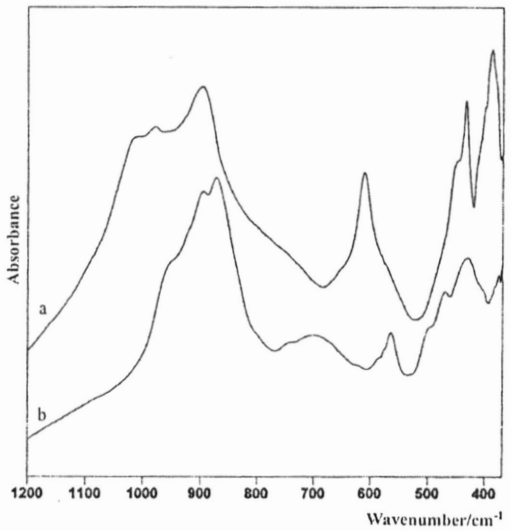

Fig. 25. Infrared spectra of zircon from Kozjak (a) and titanite from Dunje (b)

Table 26

Frequencies and intensities of the bands in the powder infrared spectrum of zircon from Kozjak compared with the corresponding literature data (in cm^{-1})

This work	Dawson *et al.*[a,b] [74]	Hubin and Tarte [75]	Nicodom[c] [60]	Rossman[c,d] [76]	Assignment[e]
388 m	389	390		390 m	"Si vs Zr" translations
400 sh	393	400		400 sh	ν_4
434 m	430	436	440 w	438 m	ν_4
450 sh	–	–	–	455 w	ν_2
611 s	608	615	612 s	610 s	ν_4
898 s	885	905	895 s	895 s	ν_3
979 w	989	1000	980 sh	980 w	ν_3
1014 sh	1008	–	1010 sh	1015 sh	ν_3

[a] Single crystal.
[b] Transverse modes are given.
[c] Wavenumbers and intensities are approximate because they are not given explicitly.
[d] Additional medium band is observed around 320 cm^{-1}.
[e] According to Dawson *et al.* [74] except the shoulder at 450 cm^{-1}.

The second step in the identification of the zircon mineral sample is the study of its Raman spectra recorded with the 1064 and 514 nm excitation lines (Fig. 26) [21]. Except for the higher background and the worse baseline of the spectrum recorded with the higher wavelength excitation line, in general, both spectra are identical and correspond to the Raman spectrum of mineral zircon studied by Calligaro *et al.* [85] (Table 27). It confirms the conjecture made by the use of IR spectroscopy that the studied sample belongs to the mineral zircon.

The previously obtained strong indications by the vibrational (IR and Raman) spectroscopy that the studied mineral sample from Kozjak is zircon were unequivocally proven by the study of its powder X-ray diagram [69] (Fig. 27) which was found to correspond to the literature data for the mineral zircon [89] (Table 28). An exception are the four weak peaks with *d*-values of 2.9891, 2.6881, 2.1200 and 1.6850 Å which are certainly due to the presence of some type of impurities.

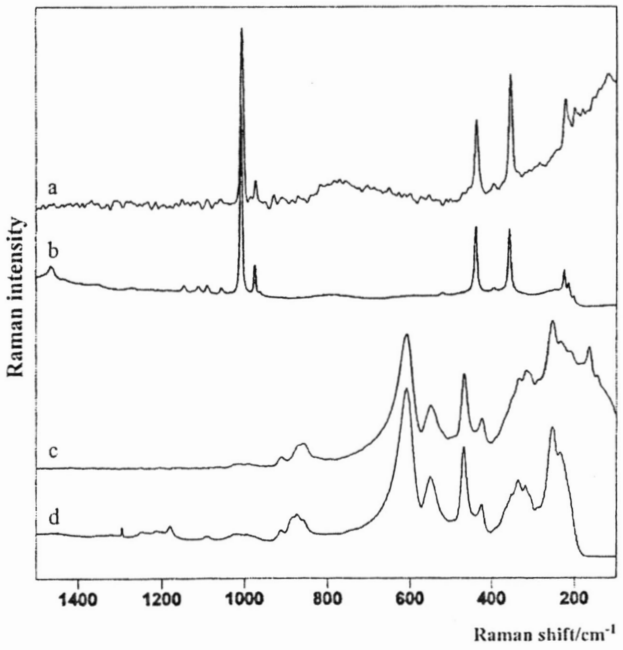

Fig. 26. Micro-Raman spectra of zircon from Kozjak (a, b) and titanite from Dunje (c, d) excited with 1064 and 514 nm lines, respectively

Table 27

Frequencies and internsity of the bands in the powder Raman spectrum of zircon from Kozjak compared with the corresponding literature data (in cm^{-1}).

This work[a,b]	This work[c]	Griffith [82]	Calligaro *et al.*[d] [85]	Assignment[e]
180 vw			180	
200 vw	200 vw		195	Zr + SiO_4 translations
–	213 vw	–	215	Zr + SiO_4 translations
224 m	224 m	–	225	
356 vs	356 s	356 vs	350	ν_2
394 vw	394 w	392 w	–	ν_2
438 s	438 s	439 s	440	ν_4
–	520 w	460 w	530	ν_4
769 m	775 vw	–	917	
973 w	973 m	975 w	979	ν_3
1008 vs	1008 vs	1010 vs	1014	ν_1

[a] Excitation with 1064 nm.
[b] Additional very weak bands appear at 1056, 1090, 1112, 1466 and 1515 cm^{-1}.
[c] Excitation with the 514 nm line.
[d] Single crystal.
[e] According to Griffith for the bands above 350 cm^{-1} [82].

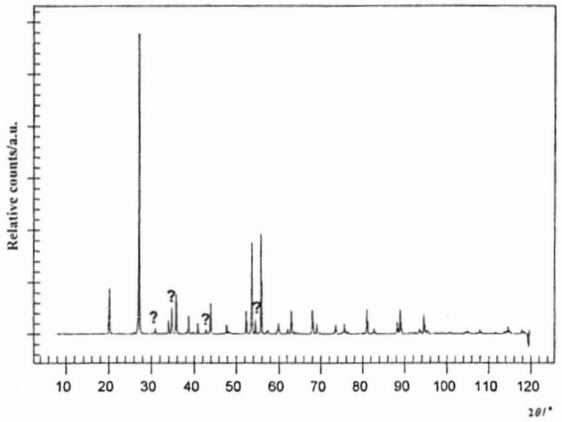

Fig. 27. Powder X-ray patterns of zircon from Kozjak. The question-marks correspond to the maxima arising from sample impurities

Table 28

The maxima in the X-ray diagram of zircon from Kozjak compared to the literature data

This work			ICDD, PDF-4 /Minerals [89]	This work			ICDD, PDF-4 /Minerals [89]
hkl	I/I_0	d_{exp} (Å)	d_{exp} (Å)	*hkl*	I/I_0	d_{exp} (Å)	d_{exp} (Å)
100	18	4.4323	4.4340	224	4	1.2589	1.2590
200	100	3.3020	3.3020	413	2	1.2484	1.2480
	2	2.9891	–	512	9	1.1884	1.1883
	10	2.6881	–	440	2	1.1674	1.1672
211	2	2.6480	2.6500	404	5	1.1080	1.1079
112	15	2.5178	2.5180	600	9	1.1007	1.1006
220	7	2.3349	2.3360	611	2	1.0682	1.0682
202	4	2.2161	2.2170	532	2	1.0591	1.0590
	2	2.1200	–	424	7	1.0508	1.0506
310	12	2.0658	2.0600	620	2	1.0440	1.0442
103	4	1.9080	1.9080	325	1	1.0013	1.0015
321	7	1.7512	1.7510	116	1	0.9745	0.9745
312	35	1.7120	1.7120	631	2	0.9714	0.9713
	5	1.6850	–	415	1	0.9582	0.9582
400	38	1.6520	1.6510	613	2	0.9534	0.9532
411	4	1.5472	1.5470	701	1	0.9319	0.9321
004	2	1.4947	1.4950	440	1	0.9201	0.9201
420	9	1.4770	1.4774	640	3	0.9158	0.9157
332	9	1.3806	1.3810	316	1	0.8993	0.8994
204	4	1.3617	1.3620	552	3	0.8915	0.8915
431	4	1.2897	1.2900				

Titanite

The IR spectrum of the studied titanite sample from Dunje (Fig. 25) is practically identical with the corresponding published (but not discussed) spectrum of this mineral [60] (Table 29). It should be pointed out that the ν_3 mode of the SiO_4 groups is split into three components (953, 897 and 873 cm^{-1}), this being very close to the literature data. Triple splitting was also observed for the ν_4 mode (566, 472 and 432 cm^{-1}), compared to the two components found in the literature [60] in the same spectral region. The broad band at 700 cm^{-1} (Fig. 25

and Table 29) is probably due to the vibrations of the TiO_6 octahedra present in the structure [21].

As seen from the practically identical Raman spectra of the titanite sample from Dunje recorded with the 1064 and 514 nm excitation lines (Fig. 25), six fundamental bands due to the silicate modes are observed in the high frequency 1000–400 cm^{-1} region (Table 30). They are in correspondence with the literature data [82, 86]. The very strong band at 608 cm^{-1}, which according to Griffith [82] does not originate from the vibrations within the silicate tetrahedra, probably arises from the Ti–O stretching vibration of the TiO_6 octahedra [21]. The remaining bands in the Raman spectrum of the studied titanite sample from Dunje (those below 400 cm^{-1}) are also in agreement with the data published by Salje *et al.* [86], contributing to the successful identification of the titanite mineral specimen. That one was indeed dealing with titanite was further proven by the great similarity of the powder X-ray diagram of the studied sample (Fig. 28 and Table 31) with the corresponding diagram of the authentic titanite mineral [89].

Table 29

Frequencies and intensities of the bands in the powder infrared spectrum of titanite from Dunje compared with the corresponding literature data (in cm^{-1})

This work	Nicodom[a] [60]	Assignment
377 vw		ν_2
407 sh	407 sh	ν_2
432 s	438 s	ν_4
472 w	–	ν_4
500 sh	–	
566 s	564 m	ν_4
578 sh	582 sh	
586 sh	–	
623 sh	617 vw	
700 m	710 vw	
744 sh	748 w	
873 s	868 s	ν_3
897 s	897 s	ν_3
953 sh	957 s	ν_3

[a] Wavenumbers and intensities are approximate because they are not given explicitly.

Table 30

Frequencies and intensities of the bands in the Raman spectrum of titanite from Dunje compared with the corresponding literature data (in cm^{-1})

This work[a]	This work[b]	Griffith [82]	Salje *et al.*[c] [86]	Assignment[d]
			75 m	
			110 m	
146 vw			140 s	
164 w			170 s	
208 sh			–	
233 vw	233 vw		230 vw	
253 m	253 m		250 vs	
286 sh	286 sh		280 w	
			310 m	
316 w	317 w		325 w	
333 vw	334 vw		340 m	
425 w	424 w	425	415 w	ν_4
467 s	468 s	467	455 s	ν_4
548 m	549 m	548	530 s	ν_4
608 vs	607 vs	608	595 vs	
856 m	856 m	856	860 vw	ν_1
872 m	873 m	874	880 w	ν_3
912 w	911 w	920	915 vw	ν_3

[a] Excitation with the 1064 nm line (Fig. 26, c).
[b] Excitation with the 514 nm line (Fig. 26, d).
[c] Wavenumbers and intensities are approximate because they are not given explicitly.
[d] According to Griffith [82].

However, impurities are undoubtedly present in the studied sample, being manifested by the appearance of the weak maxima (with *d*-values of 8.226, 3.6144, 1.6061, 1.4355 and 1.2393 Å; cf. Table 31) which are not mentioned in the literature [89].

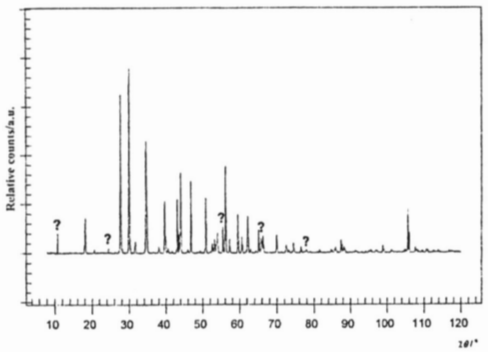

Fig. 28. Powder X-ray patterns of titanite from Dunje. The question-marks correspond to the maxima arising from sample impurities

Table 31

The maxima in the X-ray diagram of titanite from Dunje compared to the literature data

This work			ICDD, PDF-4 Minerals [89]	This work			ICDD, PDF-4 /Minerals [89]
hkl	I/I_0	d_{exp} (Å)	d_{exp} (Å)	*hkl*	I/I_0	d_{exp} (Å)	d_{exp} (Å)
	12	8.226	–		10	1.6061	–
–111	19	4.9396	4.930	241	20	1.5591	1.5540
	5	3.6144	–	043	11	1.5323	1.5270
002	70	3.2313	3.2330	133	17	1.4974	1.4940
–202	100	2.9970	2.9890		14	1.4355	–
200	7	2.8491	2.8410	061	9	1.4180	1.4180
022	52	2.5961	2.5950	–225	10	1.4068	1.4090
–113	7	2.3655	2.3620	223	12	1.3445	1.3440
112	26	2.2731	2.2730	–262	7	1.3089	1.3060
131	6	2.2360	2.2250	–135	8	1.2770	1.2750
–312	28	2.1098	2.1010		5	1.2393	–
041	55	2.0656	2.0580	–245	5	1.2280	1.2270
221	5	1.9859	1.9720	–531	9	1.1339	1.1320
–313	34	1.9476	1.9450	–335	10	1.1083	1.1070
–204	4	1.8537	1.8480	–535	9	1.1083	1.1070
042	26	1.8072	1.8020	006	5	1.0771	1.0770
–332	12	1.7411	1.7410	370	5	1.0417	1.0420
240	10	1.7313	1.7350	–536	4	1.0294	1.0300
–224	13	1.7059	1.7030	173	6	1.0146	1.0150
–333	44	1.6465	1.6430	–606	5	0.9990	0.9990

Olivines

As has already been mentioned, the term olivine, $(Mg,Fe)_2SiO_4$, is used for solid solutions of the isomorphous forsterite, Mg_2SiO_4, and fayalite, Fe_2SiO_4.

The IR spectra of the above-mentioned two minerals are discussed by various authors [60, 71, 77, 78] and are rather similar. In order to compare them with the IR spectrum of the studied [21] olivine sample from 'Ržanovo (Fig. 29), the obtained data are summarized in Table 32. It should be pointed out that, according to Burns and Huggins [78], all IR bands of the forsterite–fayalite series show a frequency shift of peak maxima to lower values with increasing iron content. This provides an opportunity to discriminate between forsterite and fayalite as well as to determine the olivine composition from the IR spectra. The application of this criterion to the IR spectrum of the olivine sample studied by us showed that the band frequencies are closer to the corresponding bands in the spectrum of forsterite, Mg_2SiO_4 (Table 32). The presence of two strong bands (at 417 and 608 cm^{-1}) in the IR spectrum of forsterite, absent in the spectrum of fayalite, may serve as a further aid in discriminating between the two end members of the olivine series. (Table 32). The lack of bands below 450 cm^{-1} in the spectrum of fayalite which are present in the spectrum of forsterite is an additional discriminating feature.

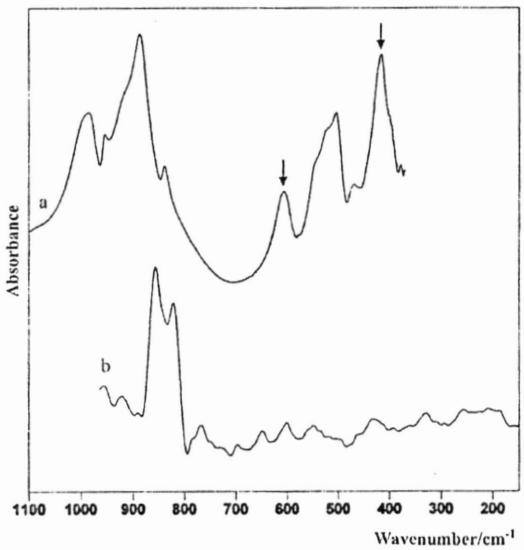

Fig. 29. Infrared (a) and micro-Raman (b) spectrum of olivine from 'Ržanovo (var. forsterite)

Table 32

Frequencies and intensities of the bands in the powder infrared spectrum of olivine From 'Ržanovo compared with the corresponding literature data (in cm^{-1})

This work	Nicodom[a] [60]	Tarte [77]		Burns & Huggins [78]		Moenke [71]	Assignment[b]
		Mg_2SiO_4	Fe_2SiO_4	Mg_2SiO_4	Fe_2SiO_4		
379 vw		380 vw	–	378 vw	–	–	
401 sh	399 s	402 sh	–	399 vw	–	–	
417 vs	–	422 s	420 sh	415 vs	–	418 s	ν_2
470 w	470 m	465 m	481 s	469 w	472 s	475 w	
505 vs	504 s	510 vs	509 m	506 vs	506 m	516 s	ν_4
522 sh	523 sh	–	–	–	–	–	
547 sh	550 sh	–	–	–	–	–	
577 vw	–	–	566 s	–	558 vs	–	
608 s	607 s	615 s	–	605 s	–	–	ν_4
839 w	838 w	842 w	832 m	838 w	827 w	848 m	ν_1
886 vs	888 vs	892 vs	879 vs	885 vs	872 vs	–	ν_3
915 sh	914 sh	–	920 w	–	914 w	898 s	
955 w	956 vw	964 w	945 sh	954w	945 s	950 w	
982 vs	982 s	990 s	963 sh	982 vs	–	–	ν_3
1000 sh	1001 sh	1001 sh	–	–	–	1002 m	ν_3

[a] Wavenumbers and intensities are approximate because explicit numerical data are not given.
[b] According to Tarte [77].

The successful identification by IR spectroscopy of the studied mineral as forsterite was, to some extent, supported by the appearance of its low-quality Raman spectrum (Fig. 29). Namely, the strongest peaks observed in the studied Raman spectrum at 823 and 855 cm–1 [21] correspond to the most intense bands registered in the literature at almost the same frequencies for forsterite [82, 87], (Table 33).

Additional similarities between the Raman spectrum of the studied sample and the corresponding spectrum of forsterite (rather than that of fayalite) were observed as well (Table 33).

The comparison of the literature powder X-ray diagrams of forsterite and fayalite [89], on the one hand, and of the studied sample, on the other hand (Fig. 30), as well as the registered complete agreement of the powder X-ray diffraction data of the studied olivine specimen from 'Ržanovo with the corresponding diagram of forsterite in [89] (Table 34) undoubtedly proves that the studied olivine sample is, in fact, forsterite in which a small amount of fayalite may be present.

Table 33

Frequencies and intensities of the bands in the powder Raman spectrum of olivine (var. forsterite) from 'Ržanovo compared with the corresponding literature data (in cm^{-1})

This work[a]	Griffith [82]		Guyot *et al.*[b]	Assignment[c]
	Mg_2SiO_4	Fe_2SiO_4	[87]	
207 w	–	–		
255 w	–	–		
329 w	327	–		ν_2
394 vw	380	380		ν_2
431 w	–	–		
463 vw	465	–		ν_4
546 w	546	550		ν_4
601 w	602	608		ν_4
648 w	–	–		
696 w	–	–		
766 w	–	–		
823 vs	823	828	824	ν_1
855 vs	860	–	855	ν_3
920 w	–	–	920	
954 w	950	–	960	ν_3

[a] Excitation with the 1064 nm line.
[b] Only the stretching SiO_4 modes are discussed.
[c] According to Griffith [82].

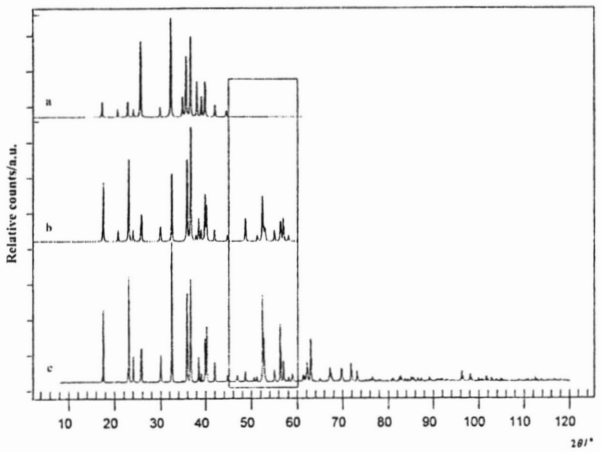

Fig. 30. Powder X-ray patterns of fayalite (a), forsterite (b) and the studied olivine sample from 'Ržanovo (c)

Table 34

The maxima in the X-ray diagram of the studied olivine sample (var. forsterite) from 'Ržanovo compared to the corresponding forsterite literature data

This work			ICDD, PDF-4 /Minerals [89]	This work			ICDD, PDF-4 /Minerals [89]
hkl	I/I_0	d_{exp} (Å)	d_{exp} (Å)	*hkl*	I/I_0	d_{exp} (Å)	d_{exp} (Å)
020	50	5.1035	5.1000	132	7	2.0723	2.0320
110	10	4.3125	4.3000	150	10	1.8760	1.8760
021	74	3.8842	3.8830	151	7	1.7902	1.7850
102	20	3.7252	3.7230	222	67	1.7497	1.7500
111	10	3.4994	3.4960	240	33	1.7401	1.7400
120	25	3.4801	3.4780	123	8	1.7314	1.7310
121	22	3.0090	3.0070	241	11	1.6710	1.6710
002	10	2.9940	2.9920	061	45	1.6364	1.6360
130	100	2.7676	2.7680	232	10	1.6338	1.6340
131	59	2.5122	2.5120	133	17	1.6190	1.6190
112	71	2.4594	2.4580	152	7	1.5897	1.5900
200	5	2.3790	2.3830	004	15	1.4970	1.4970
041	20	2.3475	2.3470	062	31	1.4791	1.4790
210	9	2.3169	2.3160	331	12	1.3978	1.3970
122	31	2.2697	2.2690	312	9	1.3885	1.3880
140	38	2.2488	2.2500	322	12	1.3515	1.3510
211	16	2.1608	2.1610	134	16	1.3167	1.3160

Kyanite

At least two clearly isolated band regions were observed in the IR spectrum of the mineral believed to be kyanite (Fig. 31).

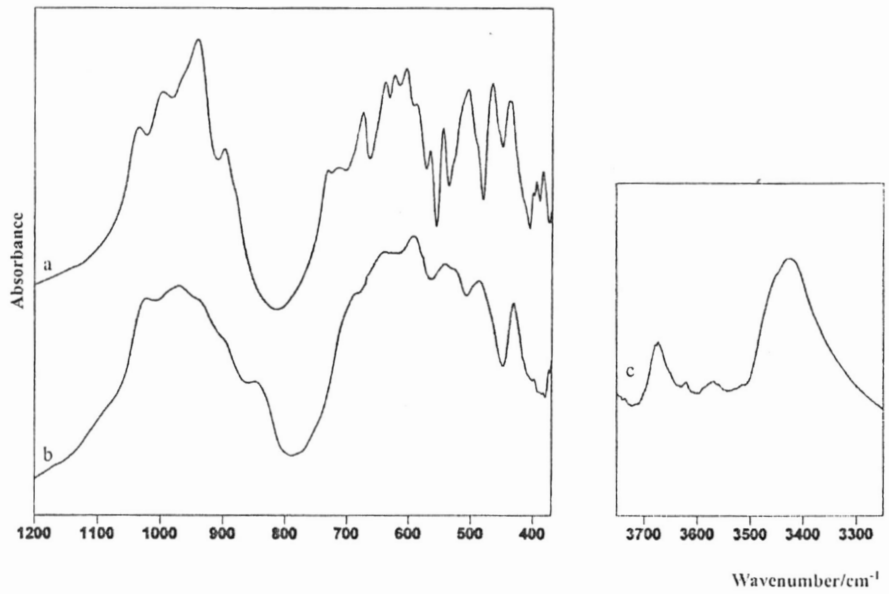

Fig. 31. Infrared spectra of kyanite from Štavica (a) and staurolite from Štavica (b, c). The band intensities between spectrum b and c are not directly comparable

The four highest frequency bands in the 1100–800 cm^{-1} region are due to the stretching SiO_4 vibrations (Table 35, Fig. 31) [21]. It should be pointed out that, contrary to all other studied nesosilicates, the IR spectrum of kyanite shows an extremely large number of bands in the region below 800 cm^{-1}, where 17 maxima appear. The strong absorption and the band frequency increase in the IR spectrum of kyanite are explained by the following structural factors: (i) the smaller Si–O–Al bond angles in kyanite (124.5 °) which causes the more pronounced Al–O stretching character of the O–Si–O bendings, and (ii) short Al–O distances (1.81–1.86 Å) [80]. According to Farmer [48], the five highest frequency bands (those from 620 to 730 cm^{-1}) can be assigned as SiO_4 bending vibrations. In any case, the comparison of the IR band frequencies of kyanite with the corresponding published (but not discussed) data [60], undoubtedly confirms the identification of this mineral as kyanite.

Table 35

Frequencies and intensity of the bands in the powder IR and Raman pectrum of kyanite from Štavica compared with the corresponding literature data (in cm^{-1})

Infrared			Raman		
This work	Nicodom[a] [60]	Assignment[b]	This work	Mernagh & Liu [88]	Assignment[c]
384 w					
395 vw				302	
400 vw			290 w		
438 m	436 w		303 vw	325	
–	440 w		314 m		
467 m	466 m		338 m		
491 sh	490 sh		354 vw	360	
505 m	503 m		373 m	386	
529 sh	–		398 m		
546 w	543 w		405 m	405	
567 vw	564 vw		417 s	419	
589 vw	588 sh		432 w	437	
605 w	603 ww		451 s		
623 w	623 vw	$\nu_{bending}(SiO_4)$	460 vw		
638 w	638 vw	$\nu_{bending}(SiO_4)$	477 vw	486	
675 m	675 w	$\nu_{bending}(SiO_4)$	499 vs		
713 w	710 sh	$\nu_{bending}(SiO_4)$	524 w		
732 vw	732 vw	$\nu_{bending}(SiO_4)$	575 m	562	
898 w	897 w	$\nu_{stretching}(SiO_4)$	618 w		$\nu_{bending}(SiO_4)$
941 m	940 s	$\nu_{stretching}(SiO_4)$	650 w		$\nu_{bending}(SiO_4)$
997 m	1002 m	$\nu_{stretching}(SiO_4)$	668 w	669	$\nu_{bending}(SiO_4)$
1035 s	1037 m	$\nu_{stretching}(SiO_4)$	902 m		$\nu_{stretching}(SiO_4)$
			911 m		$\nu_{stretching}(SiO_4)$
			964 s	952	$\nu_{stretching}(SiO_4)$
			970 s		$\nu_{stretching}(SiO_4)$
			1013 m		$\nu_{stretching}(SiO_4)$

[a] Wavenumbers and intensities are approximate because they are not given explicitly.
[b] Vibrational modes from the SiO_4 tetrahedra according to Farmer [48].
[c] According to Griffith [82].

The appearance of an extremely large number of bands is also characteristic of the Raman spectrum of kyanite (Fig. 32 and Table 35). Similarly to the above discussion regarding the IR spectrum, the five highest frequency bands in the 1015–900 cm^{-1} region are ascribed to the split bands arising from the SiO_4 stretching modes ν_3 and ν_1. The remaining three bands at the lower frequency (in the 670–620 cm^{-1}) region are attributed to the SiO_4 bending ν_4 modes also split into three components.

The above discussion of the IR and Raman spectra of kyanite shows that the vibrations of the SiO_4 groups dominate, implying that there are weak interactions between the AlO_6 octahedra and the silicate tetrahedra [88].

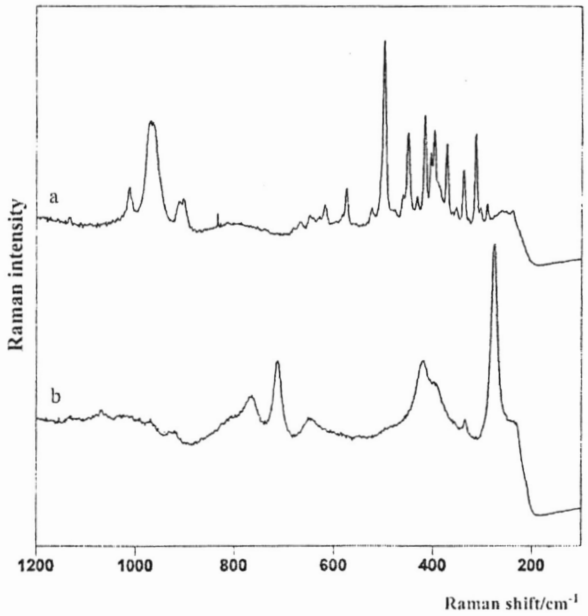

Fig. 32. Micro-Raman spectra of kyanite from Štavica (a) and staurolite from Štavica (b) excited with 514 nm line

The definite identification of the kyanite mineral sample from Štavica by vibrational spectroscopy is additionally confirmed by the complete agreement of the powder X-ray diagram of the studied sample (Fig. 33) with the corresponding literature data [89] (Table 36). No additional maxima were observed in the studied diagram [89].

Table 36

The maxima in the X-ray diagram of the studied kyanite sample from Štavica compared to the corresponding kyanite literature data

This work			ICDD, PDF-4 /Minerals [89]	This work			ICDD, PDF-4 /Minerals [89]
hkl	I/I_0	d_{exp} (Å)	d_{exp} (Å)	*hkl*	I/I_0	d_{exp} (Å)	d_{exp} (Å)
010	23	7.5458	7.5463	301	19	1.9380	1.9375
100	11	6.7081	6.7085	–302	44	1.9305	1.9302
011	20	4.3102	4.3126	0–32	20	1.9063	1.9050
–111	15	4.3014	4.3126	–322	13	1.8788	1.8809
–1–11	23	3.7712	3.7708	1–41	11	1.8501	1.8495
–210	17	3.4441	3.4440	–411	30	1.7639	1.7639
200	78	3.3540	3.3542	013	17	1.7482	1.7488
–121	60	3.1870	3.1831	132	15	1.6095	1.6104
021	18	3.0246	3.0263	–422	19	1.5914	1.5899
120	29	2.9536	2.9507	–4–11	12	1.5725	1.5724
–1–21	13	2.7568	2.7526	0–33	11	1.5177	1.5169
–2–11	36	2.6975	2.6970	–151	16	1.5034	1.5039
–130	12	2.6077	2.6076	0–51	14	1.4767	1.4763
030	52	2.5153	2.5154	123	23	1.4658	1.4665
121	14	2.4647	2.4659	–350	15	1.4541	1.4540
1–31	35	2.3372	2.3362	–511	14	1.4151	1.4151
–310	16	2.3291	2.3291	213	13	1.4089	1.4094
–122	12	2.2731	2.2742	150	10	1.3912	1.3914
–320	23	2.2151	2.5174	3–42	13	1.3799	1.3794
–321	29	2.1818	2.1820	–2–42	70	1.3784	1.3779
–2–12	14	2.1658	2.1644	–442	26	1.3760	1.3763
1–22	29	2.1572	2.1563	–522	17	1.3473	1.3474
–3–11	21	2.0052	2.0050	500	100	1.3416	1.3417
221	61	1.9449	1.9457	–1–52	12	1.2902	1.2896

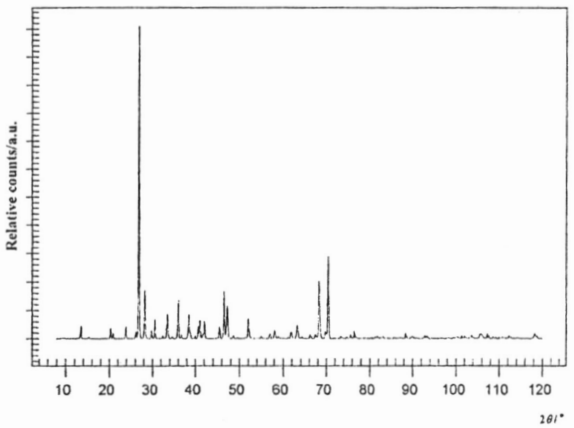

Fig. 33. Powder X-ray patterns of kyanite sample from Štavica

Staurolite

The IR spectrum of staurolite (Fig. 31) shows, to some extent, similarities with the corresponding spectrum of kyanite, being characterized by the appearance of two well-separated regions [21]. The higher frequency region (1100 to 800 cm^{-1}) is represented by a very strong and complex band with the maximum at 971 cm^{-1}, accompanied by four additional weak to medium peaks or shoulders on both sides (Table 37). There is no doubt that these bands arise from the stretching vibrations of the SiO_4 units. The close similarity of the IR spectrum of the studied staurolite with the corresponding literature data is observed not only in this region, but also in the bands between 700 and 590 cm^{-1} where the SiO_4 bendings appear (Table 37).

Compared to all other studied nesosilicate minerals, only staurolite contains OH groups. Their presence in the structure of staurolite is manifested by the bands above 3400 cm^{-1} (Fig. 31) where three pairs of bands are observed: the first of them is characterized by the peaks at 3426, 3451 cm^{-1}, the second by maxima at 3520 and 3571 cm^{-1} and the third by peaks at 3622 and 3675 cm^{-1} (Table 37). As seen from Table 37, quite good agreement exists between the studied spectrum and the polarized staurolite spectra from Koch-Mülerr *et al.* [81]. According to these authors, the interpretation of the two highest frequency bands can not be based on the known proton positions for staurolite so they were assigned to an additional proton (H3), different from previously known in the structure of this mineral, H1 and H2 [81]. The appearance of our spectra may be taken as an indication that the studied staurolite sample also contains

three structurally different hydrogen atoms. Further structural studies should be carried out in order to confirm the above hypothesis. In spite of that, the identification of the studied mineral as staurolite using IR spectroscopy is beyond doubt.

Table 37

Frequencies and intensities of the bands in the powder IR spectrum of staurolite from Štavica compared with the corresponding literature data (in cm^{-1})

This work	Nicodom[a] [60]	Koch-Müller *et al.* [81] (010) E$\|c$	(010) E$\|a$	Assignment[b]
399 vw	407 vw			
432 m	433 w			
487 m	484 w			
525 sh	522 vw			
543 w	540 vw			
593 m	590 w			$\nu_{bending}(SiO_4)$
640 sh	645 vw			$\nu_{bending}(SiO_4)$
684 vw	689 sh			$\nu_{bending}(SiO_4)$
847 sh	843 w			$\nu_{stretching}(SiO_4)$
898 sh	897 w			$\nu_{stretching}(SiO_4)$
938 sh	–			$\nu_{stretching}(SiO_4)$
970 s	963 s			$\nu_{stretching}(SiO_4)$
1022 m	1022 w			$\nu_{stretching}(SiO_4)$
–	–	3340	3358	ν_{H1}
3426 s	3420 m	3424	3420	ν_{H1}
3451 sh	–	3450	3442	ν_{H1}
–	–	3468	3465	ν_{H1}
3520 sh	–	3525	3525	ν_{H2}
3571 vw	3575 w	3577	3577	ν_{H2}
3622 vw	3670 w	3635	3635	ν_{H3}
3675 m	–	3677	3677	ν_{H3}

[a] Wavenumbers and intensities are approximate because explicit numerical data are not given.
[b] According to Koch-Müller *et al.* [81] for the bands above 3000 cm^{-1}.

The Raman spectra of staurolite and kyanite are rather different (Fig. 32), contrary to the similarity between their IR spectra (Fig. 31) [21]. To the best of our knowledge, there are no literature data regarding the Raman spectrum of staurolite. This makes it more difficult to use the studied low-quality Raman spectrum for identification purposes. However, the barely observed three weak bands above 900 cm^{-1} can probably be assigned as the stretching SiO_4 vibrations (Table 38) [21]. According to the above assignment of the IR spectrum of staurolite, the bands in the 800–650 cm^{-1} spectral region can be attributed to the SiO_4 bendings.

Table 38

Frequencies and intensities of the bands in the powder Raman spectrum of staurolite from Štavica (in cm^{-1})

This work	Assignment
276 vs	
335 w	
396 sh	
419 vs	
649 m	$\nu_{bending}$ (SiO_4)
715 s	$\nu_{bending}$ (SiO_4)
767 m	$\nu_{bending}$ (SiO_4)
925 w	$\nu_{strething}$ (SiO_4)
968 w	$\nu_{strething}$ (SiO_4)
1069 vw	$\nu_{strething}$ (SiO_4)

Apart from the two wery weak peaks (at *d*-values 2.3204 and 1.4265 Å) which obviously arise from the presence of minute impurities in the sample, the powder X-ray diagram of the studied staurolite specimen (Fig. 34) corresponds completely to the literature data [89] (Table 39), undoubtedly confirming that the studied mineral is indeed staurolite.

Table 39

The maxima in the X-ray diagram of the studied staurolite sample from Štavica compared to the corresponding staurolite literature data

This work			ICDD, PDF-4 /Minerals [89]	This work			ICDD, PDF-4 /Minerals [89]
hkl	I/I_0	d_{exp} (Å)	d_{exp} (Å)	*Hkl*	I/I_0	d_{exp} (Å)	d_{exp} (Å)
110	19	7.0680	7.0681	–191	6	1.7035	1.7030
021	5	4.6408	4.6521	–223	20	1.6543	1.6586
–111	6	4.3975	4.4071	–402	5	1.6052	1.6070
040	14	4.1300	4.1300	402	14	1.6026	1.6044
220	17	3.5340	3.5340	–153	29	1.5940	1.5969
131	8	3.5145	3.5131	243	7	1.5603	1.5647
–201	18	3.2104	3.2141	063	7	1.5469	1.5507
150	7	3.0435	3.0435	–282	24	1.5309	1.5314
–221	31	2.9923	2.9911	313	8	1.5118	1.5153
002	17	2.8050	2.8150	–192	12	1.5074	1.5090
060	12	2.7533	2.7533	–442	5	1.4962	1.4977
–151	32	2.6759	2.6781	–333	5	1.4658	1.4688
–241	100	2.5347	2.5339	–391	5	1.4504	1.4505
241	25	2.5321	2.5339	263	5	1.4377	1.4408
–132	7	2.3818	2.3880		5	1.4265	–
330	15	2.3560	2.3560	010.2	5	1.4235	1.4248
–311	6	2.3416	2.3431	550	7	1.4136	1.4136
–202	14	2.2810	2.2864	004	6	1.4026	1.4075
170	13	2.2594	2.2594	462	17	1.3850	1.3862
260	13	2.2512	2.2512	–353	10	1.3841	1.3841
	5	2.3204	–	–481	5	1.3767	1.3767
–171	11	2.0961	2.0972	–204	5	1.3209	1.3250
062	14	1.9649	1.9683	620	5	1.2874	1.2874
400	16	1.9550	1.9550	154	5	1.2741	1.2772
003	11	1.8700	1.8767	–621	9	1.2553	1.2555
190	6	1.7870	1.7870	064	6	1.2497	1.2532
–281	7	1.7367	1.7365				

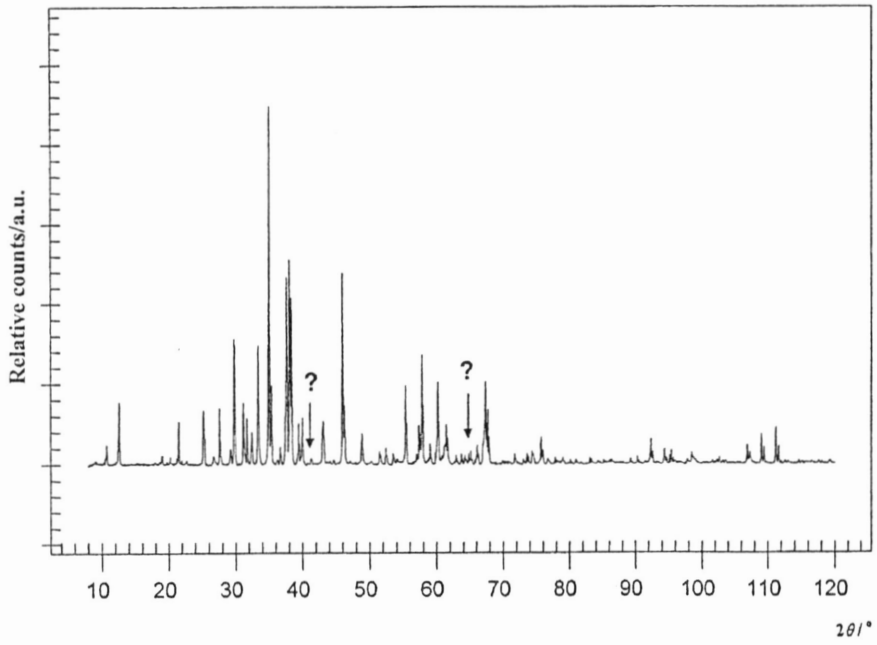

Fig. 34. Powder X-ray patterns of staurolite sample from Štavica. The question-marks correspond to the maxima arising from sample impurities

4. CONCLUSIONS

The study of the carbonate minerals by FT IR spectroscopy has shown that this technique is suitable for distinguishing some rhombohedral calcite type minerals which essentially share the same structure. This is mainly due to the marked sensitivity of the ν_4 vibrational mode to the change of divalent cation size [$r(Ca^{2+}) > r(Fe^{2+}) > r(Mg^{2+})$] in calcite, siderite and magnesite minerals, respectively. The most pronounced frequency difference between the corresponding ν_4 modes in magnesite and calcite is large enough (36 cm^{-1}) and makes it possible to detect the presence of very low content (1 wt %) of magnesite in calcite and vice versa. On the other hand, the appearance of the ν_1 mode in the IR spectrum of aragonite (at 1083 cm^{-1}, absent in the spectrum of calcite) serves as a basis for detecting the presence of small amounts of aragonite in calcite (1 wt %). The determination of the impurities of calcite in aragonite by powder X-ray diffraction and vice versa has shown that the limit of detection of the presence of aragonite in calcite is around 1 wt %, whereas the lower limit of

detection of aragonite in calcite is about 0.5 wt %. The comparison of the obtained data regarding the determination of impurities of calcite in aragonite and vice versa shows that, in the present case, powder X-ray diffraction is a more accurate method than IR spectroscopy, but this should not be taken as a general conclusion, because the determination of the low limit of the impurities present varies from case to case.

The vibrational (IR and Raman) spectra as well as the powder X-ray diffraction patterns enable a rapid check on the purity of the sulfide minerals galena, sphalerite and wurtzite and give an unambiguous opportunity for their identification. During this process, some problems can arise: (a) the presence of impurities in the studied samples; (b) the decomposition of the sample during the process of spectrum recording; (c) the transformation of one mineral form to another one, etc. Therefore, the application of the three most frequently used instrumental techniques (IR and Raman vibrational spectroscopy and powder X-ray diffracttion) for mineral identification and characterization does not necessarily and unequivocally enable discrimination between minerals which often appear together and may undergo transformation from one to the other form.

Both far and mid IR spectra are useful for the study of the oxide minerals because, for some of them, absorption bands in the higher frequency region are observed. Therefore, the IR spectra in both regions can serve as a powerful qualitative tool for oxide mineral identification and characterization purposes. It should be pointed out that the problems concerning the particle size and form as well as sample powdering and preparation should not be underestimated for acquiring high-quality spectra. In some cases, significant disagreement between various IR literature data for the same mineral (e. g. limonite) may cause additional difficulties in the course of identification of the studied minerals. On the other hand, the powder X-ray diffraction technique enables a rapid check on the purity of the studied oxide minerals, giving an unambiguous opportunity for their identification. Although both techniques are complementary rather than competitive, the analysis of the oxide minerals proves that the powder X-ray diffraction is more sensitive to the determination of mineral impurities compared to the FT IR spectroscopy.

The identification of the nesosilicate minerals almandine, spessartine, zircon, titanite and kyanite by vibrational (IR and Raman) spectroscopy is undisputed, whereas some difficulties appear in the process of the identification of the staurolite and olivine (forsterite and fayalite) mineral specimens because of the lower quality of their Raman spectra recorded by us. On the other hand, one should be aware that some structural changes in the mineral may occur during the Raman experiment performed by using different excitation lines (as in

the case of the studied almandine specimen). Generally, in the case of nesosilicates, IR spectroscopy is a more powerful technique for mineral identification compared to the Raman experiment. The identification difficulties caused by the low quality of our Raman spectra as well as by the presence of impurities in some of the studied samples are overcome by the investigation of the powder X-ray diffraction diagrams of the nesosilicate mineral specimens.

Acknowledgment. The financial support from the Ministry of Education and Science of the Republic of Macedonia is gratefully acknowledged.

REFERENCES

[1] M. Trajkovska, B. Šoptrajanov, G. Jovanovski, T. Stafilov, *J. Mol. Struct.*, **267**, 191 (1992).

[2] M. Trajkovska, B. Šoptrajanov, T. Stafilov, G. Jovanovski, *Geologica Macedonica*, **7**, 55 (1993).

[3] B. Šoptrajanov, M. Trajkovska, I. Gržetić, G. Jovanovski, T. Stafilov, *N. Jb. Miner. Abh.*, **166**, 83 (1993).

[4] B. Šoptrajanov, M. Trajkovska, G. Jovanovski, T. Stafilov, *N. Jb. Miner. Abh.*, **167**, 329 (1994).

[5] B. Šoptrajanov, M. Trajkovska, T. Stafilov, G. Jovanovski, I. Gržetić, *Spectrosc. Lett.*, **30**, 79 (1997).

[6] G. Jovanovski, V. Stefov, B. Jovanovski, B. Šoptrajanov, B. Kaitner, *16th Congress of Chemists and Technologists of Macedonia, Book of Papers*, Skopje, 1999, p. 43.

[7] V. Stefov, S. Dimitrovska, G. Jovanovski, B. Šoptrajanov, *16th Congress of Chemists and Technologists of Macedonia, Book of Papers*, Skopje, 1999, p. 47.

[8] G. Jovanovski, V. Stefov, B. Jovanovski, B. Šoptrajanov, B. Boev, *Geologica Macedonica*, **13**, 69 (1999).

[9] V. Stefov, G. Jovanovski, B. Šoptrajanov, B. Minčeva-Šukarova, S. Dimitrovska, B. Boev, *Geologica Macedonica*, **14**, 61 (2000).

[10] P. Makreski, G. Jovanovski, V. Stefov, B. Minčeva-Šukarova, B. Kaitner, B. Boev, *Geologica Macedonica*, **15–16**, 43 (2001–2002).

[11] B. Boev, V. Bermanec, T. Serafimovski, S. Lepitkova, S. Mikulčić, M. Šoufek, G. Jovanovski, T. Stafilov, M. Najdoski, *Geologica Macedonica*, **15**, 1 (2001).

[12] G. Jovanovski, B. Minčeva-Šukarova, P. Makreski, B. Šoptrajanov, W. P. Griffith, R. L. Willis, *Eighteenth International Conference on Raman Spectroscopy, Proceedings*, Budapest, 2002, p. 931.

[13] G. Jovanovski, B. Minčeva-Šukarova, P. Makreski, V. Stefov, W. P. Griffith, R. L. Willis, *Eighteenth International Conference on Raman Spectroscopy, Proceedings*, Budapest, 2002, p. 933.

[14] G. Jovanovski, V. Stefov, B. Šoptrajanov, B. Boev, *N. Jb. Miner. Abh.*, **177**, 241 (2002).

[15] B. Minceva-Sukarova, G. Jovanovski, P. Makreski, B. Soptrajanov, W. P. Griffith, R. L. Willis, I. Grzetic, *J. Mol. Struct.*, **651–653**, 181 (2003).

[16] P. Makreski, G. Jovanovski, *Bull. Chem. Technol. Macedonia*, **22**, 25 (2003).

[17] G. Jovanovski, B. Boev, P. Makreski, M. Najdoski, G. Mladenovski, *Bull. Chem. Technol. Macedonia*, **22**, 111 (2003).

[18] P. Makreski, G. Jovanovski, B. Minceva-Sukarova, B. Soptrajanov, A. Green, B. Engelen, I. Grzetic, *Vib. Spectrosc.*, **35**, 59 (2004).

[19] P. Makreski, G. Jovanovski, B. Kaitner, T. Stafilov, B. Boev, D. Cibrev, *N. Jb. Miner. Abh.*, **180**, 215 (2004).

[20] P. Makreski, G. Jovanovski, T. Stafilov, B. Boev, *Bull. Chem. Technol. Macedonia*, **23**, 171 (2004).

[21] P. Makreski, G. Jovanovski, S. Stojančeska, *J. Mol. Struct.*, **744–747**, 79 (2005).

[22] P. Makreski, G. Jovanovski, S. Dimitrovska, *Vib. Spectrosc.*, **39**, 229 (2005).

[23] P. Makreski, G. Jovanovski, A. Gajović, *Vib. Spectrosc.*, **40**, 98 (2006).

[24] T. Stafilov, A. Lazaru, E. Pernicka, *Acta Chim. Slo.*, **40**, 37 (1993).

[25] T. Stafilov, A. Lazaru, E. Pernicka, *At. Spectrosc.*, **16**, 158 (1995).

[26] A. Lazaru, T. Stafilov, *Fresenius' J. Anal. Chem.*, **360**, 726 (1998).

[27] T. Stafilov, *Spectrochim. Acta,* **B55**, 893 (2000).

[28] D. Zendelovska, T. Stafilov, B. Boev, *Geol. Macedonica*, **14**, 67 (2000).

[29] D. Zendelovska, T. Stafilov, *Anal. Sci.*, **17**, 425 (2001).

[30] D. Zendelovska, G. Pavlovska, K. Čundeva, T. Stafilov, *Talanta*, **54**, 139 (2001).

[31] T. Stafilov, D. Zendelovska, *Turkish J. Chem.*, **26**, 271 (2002).

[32] A. Lazaru, R. Jaćimović, R. Ilić, D. Mihajlović, T. Stafilov, *J. Radioanal. Nucl. Chem.*, **253**, 427 (2002).

[33] T. Stafilov, D. Zendelovska, G. Pavlovska, K. Čundeva, *Spectrochim. Acta,* **B57**, 907 (2002).

[34] P. Makreski, V. Paneva, G. Jovanovski, T. Stafilov, D. Zendelovska, *3rd Aegean Analytical Chemistry Days*, *Proceedings*, Polihnotos, Lezvos, 2002, p. 440.

[35] N. Angelov, T. Stafilov, *Geol. Macedonica*, **17**, 73 (2003).

[36] V. Zajkova, T. Stafilov, B. Boev, *Geol. Macedonica*, **17**, 87 (2003).

[37] G. Pavlovska, K. Čundeva, T. Stafilov, D. Zendelovska, *Sep. Sci. Technol.*, 38, 1117 (2003).

[38] T. Stafilov, N. Angelov, R. Jaćimović, V. Stibilj, *Microchim. Acta*, 149, 229 (2005).

Прилози, Одд. мат. тех. науки, **XXVI**, 1 (2005), с. 7–84

[39] V. Zajkova Paneva, K. Cundeva, T. Stafilov, *Spectrochim. Acta*, **B60**, 403 (2005).

[40] D. Bish, J. Post, *Am. Mineral.*, **78**, 932 (1993) and references therein.

[41] V. C. Farmer, Sixth Ceramic Chemists' Conference (on Silicate Analysis), *Spec. Publ.* No. **98**, 101 (1979).

[42] W. P. Griffith in V. C. Farmer (Ed.), *The Infrared Spectra of Minerals,* Mineralogical Society, London, 1974, p. 119.

[43] E. A. Moldowski, D. J. Morgan, *Nature*, **286**, 248 (1980) and references therein.

[44] S. J. Gaffey, *Am. Mineral.*, **71**, 151 (1986) and references therein.

[45] W. D. Nesse, *Introduction to Mineralogy*, Oxford University Press, New York, 2000.

[46] M. S. Freedman, C. M. Stevens, E. P. Honwitz, L. H. Fuchs, J. Sherner, L. S. Goodman, W. J. Childs, *Science*, **193**, 1117 (1976).

[47] M. K. Pavičević, *Nucl. Instrum. Meth.*, **A271**, 287 (1988).

[48] V. C. Farmer (Ed.), *The Infrared Spectra of Minerals*, Mineralogical Society, London, 1974.

[49] R. Soong, V. C. Farmer, *Miner. Mag.*, **42**, 277 (1978).

[50] I. I. Plyusnina, *Infrakrasnye spektry mineralov*, Izdatel'stvo Moskovskogo universiteta, Moskva, 1977.

[51] L. G. Berry (Ed.), *Inorganic Index to the Powder Diffraction File*, Joint Committee on Powder Diffraction Standards, Pennsylvania, 1972.

[52] T. P. Mernagh, A. G. Trudu, *Chem. Geol.*, **103**, 113 (1993).

[53] V. Bermanec, *Sistematska mineralogija – mineralogija nesilikata*, Targa, Zagreb, 1999.

[54] D. G. Taylor, C. M. Nenadic, J. V. Crable, *Amer. Ind. Ass. J.*, **31**, 100 (1970).

[55] N. T. McDevitt, W. L. Baun, *Spectrochim. Acta*, **20**, 799 (1964).

[56] C. J. Serna, J. L. Rendon, J. E. Iglesias, *Spectrochim. Acta*, **A 38**, 797 (1982).

[57] P. F. McMillan, A. M. Hofmeister, *Rev. Miner.*, **18**, 99 (1988).

[58] L. G. Berry, R. M. Thompson, *X-ray Powder Data for Ore Minerals*: *The Peacock Atlas*, Geological Society of America, New York, 1962.

[59] R. E. Newnham, Y. M. De Haan, *Z. Kristallogr.*, **117**, 235 (1962).

[60] Inorganic Library of FT IR Spectra – Minerals, NICODOM, 1998.

[61] H. D. Lutz, H. Haeuseler, *Trends Appl. Spectrosc.*, **2**, 59 (1998).

[62] J. T. Luxon, R. Summitt, *J. Chem. Phys.*, **50**, 1366 (1969).

[63] M. Ocana, C. J. Serna, *Spectrochim. Acta*, **A 47**, 765 (1991).

[64] A. Oles, A. Szytula, A. Wanic, *Phys. Stat. Sol.*, **41**, 173 (1970).

[65] K. Sato, T. Sudo, F. Kurosawa, O. Kammori, *Nippon Kink. Gakk.*, **33**, 1371 (1969).

[66] E. Schwarzmann, H. Sparr, *Z. Naturf.*, **B24**, 8 (1969).

[67] Ya. I. Ryskin in V. C. Farmer (Ed.), *The Infrared Spectra of Minerals,* Mineralogical Society, London, 1974, p. 137.

[68] W. B. White, R. Roy, *Am. Mineral.*, **49**, 1670 (1964).

[69] G. Jovanovski, B. Kaitner, P. Makreski, B. Boev, S. Stojančeska, *14th Croatian–Slovenian Crystallographic Meeting*, *Book of Abstracts*, Vrsar, 2005, p. 38.

[70] T. Boffa Ballaran, M. A. Carpenter, G. A. Geiger, A. M. Koziol, *Phys. Chem. Miner.*, **26**, 554 (1999).

[71] H. Moenke, *Mineralspektren*, Vol. I, Academie, Berlin, 1962.

[72] R. K. Moore, W. B. White, T. V. Long, *Am. Mineral.*, **56**, 54 (1971).

[73] A. M. Hofmeister, A. Chopelas, *Phys. Chem. Miner.*, **17**, 503 (1991).

[74] P. Dawson, M. M. Hargreave, G. R. Wilkinson, *J. Phys.*, **4C**, 240 (1971).

[75] R. Hubin, P. Tarte, *Spectrochim. Acta*, **A27**, 683 (1971).

[76] G. R. Rossman, *Trans. Am. Crystallogr. Assoc.*, **15**, 107 (1979).

[77] P. Tarte, *Spectrochim. Acta*, **19**, 25 (1963).

[78] R. G. Burns, F. E. Huggins, *Am. Mineral.*, **57**, 967 (1972).

[79] A. Beran, K. Langer, M. Andrut, *Mineral. Petrol.*, **48**, 257 (1993).

[80] P. Tarte, *Bull. Soc. Fr. Ceram.*, **58**, 13 (1963).

[81] M. Koch-Müller, K. Langer, A. Beran, *Phys. Chem. Miner.*, **22**, 108 (1995).

[82] W. P. Griffith, *J. Chem. Soc.*, **A**, 1372 (1969).

[83] B. A. Kolesov, C. A. Geiger, *J. Raman Spectrosc.*, **28**, 659 (1997).

[84] B. A. Kolesov, C. A. Geiger, *Phys. Chem. Miner.*, **25**, 142 (1998).

[85] T. Calligaro, S. Colinart, J. P. Poirot, C. Sudres, *Nucl. Instrun. Meth.*, **189B**, 320 (2002).

[86] E. Salje, C. Schmidt, U. Bismayer, *Phys. Chem. Miner.*, **19**, 502 (1993).

[87] F. Guyot, H. Boyer, M. Madon, B. Velde, J. P. Poirier, *Phys. Chem. Miner.*, **13**, 91 (1986).

[88] T. P. Mernagh, L. Liu, *Phys. Chem. Miner.*, **18**, 126 (1991).

[89] Powder Diffraction File-4/Minerals, International Center for Diffraction Data, Pennsylvania, 2005.

Р е з и м е

МИНЕРАЛИ ОД МАКЕДОНИЈА. КОМПЛЕМЕНТАРНА УПОТРЕБА НА ВИБРАЦИОНАТА СПЕКТРОСКОПИЈА И РЕНДГЕНСКАТА ДИФРАКЦИЈА НА СПРАШЕНИ ОБРАСЦИ ПРИ ИДЕНТИФИКАЦИЈАТА И ДЕТЕКЦИЈАТА

Даден е преглед на резултатите на комплементарната анализа (извршена со инфрацрвена и раманска спектроскопија и со рендгенска дифракција од спрашени обрасци) на некои карбонатни, сулфидни, оксидни и силикатни минерали што потекнуваат од Република Македонија. Анализата е вршена со цел да се идентификуваат и да се карактеризираат изучуваните минерали. Изучувани се следниве минерали: калцит, $CaCO_3$; арагонит, $CaCO_3$; сидерит, $FeCO_3$; магнезит, $MgCO_3$; доломит, $CaMg(CO_3)_2$; кутнахорит, $CaMn(CO_3)_2$; галенит, PbS; сфалерит/вурцит, (Zn,Fe)S; хематит, Fe_2O_3; магнетит, Fe_3O_4; лимонит, FeOOH; гетит, α-FeOOH; корунд, Al_2O_3; рутил, TiO_2; хромит, $FeCr_2O_4$; алмандин, $Fe_3Al_2(SiO_4)_3$; спесартин, $Mn_3Al_2(SiO_4)_3$; циркон, $ZrSiO_4$; титанит, $CaTiSiO_5$; оливин, $(Mg,Fe)_2SiO_4$; форстерит, Mg_2SiO_4; ставролит, $Fe_2Al_9O_6(SiO_4)_4(OH)_2$ и кијанит, Al_2SiO_5.

Клучни зборови: минерали, вибрациона спектроскопија, рендгенска дифракција на спрашени обрасци

Address:
Gligor Jovanovski
Institute of Chemistry, Faculty of Science, Ss Cyril and Methodius University, P.O. Box 162, MK-1001 Skopje, Republic of Macedonia
E-mail: gligor@ pmf.ukim.edu.mk

Petre Makreski
Institute of Chemistry, Faculty of Science, Ss Cyril and Methodius University, P.O. Box 162, MK-1001 Skopje, Republic of Macedonia
E-mail: petremak@iunona.pmf.ukim.edu.mk

Bojan Šoptrajanov
Macedonian Academy of Science and Art, MK-1000 Skopje, Republic of Macedonia
E-mail: bojan@manu.edu.mk

Branko Kaitner
Laboratory of General and Inorganic Chemistry, Chemistry Department, Faculty of Science, University of Zagreb, ul. kralja Zvonimira 8, HR-10002 Zagreb, Croatia
E-mail: kaitner@chem.pmf.hr

Blažo Boev
Department of Petrology, Mineralogy and Geochemistry, Faculty of Mining and Geology, Ss Cyril and Methodius University, Goce Delčev 89, MK-2000 Štip, Republic of Macedonia
E-mail: bboev@rgf.ukim.edu.mk

Contributions, Sec. Math. Tech. Sci., **XXVI**, 1 (2005), pp. 7–84

Appendix

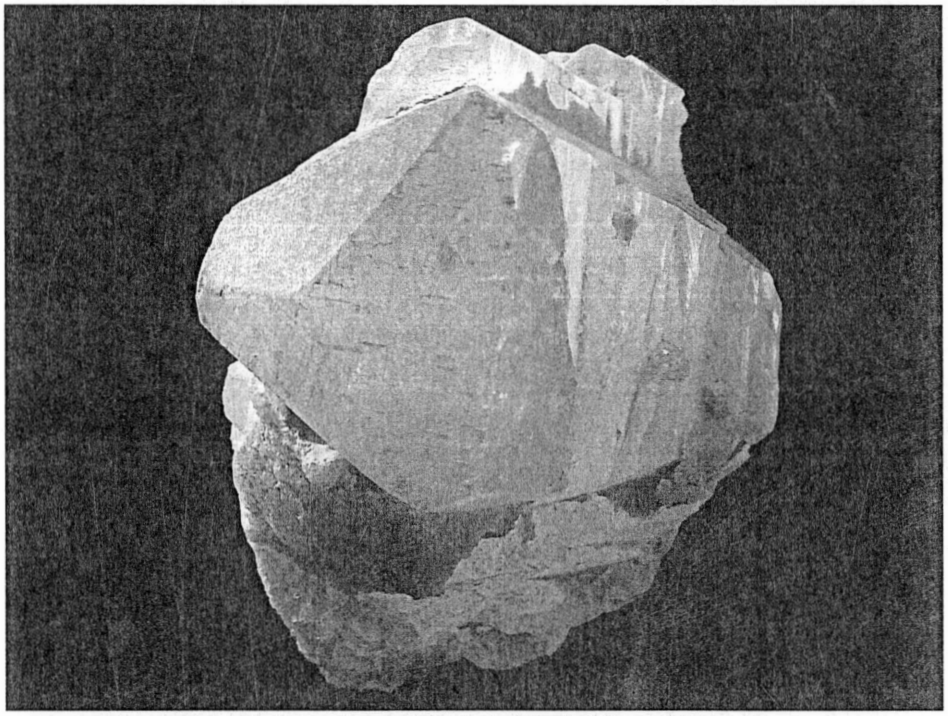

Calcite from Sivec

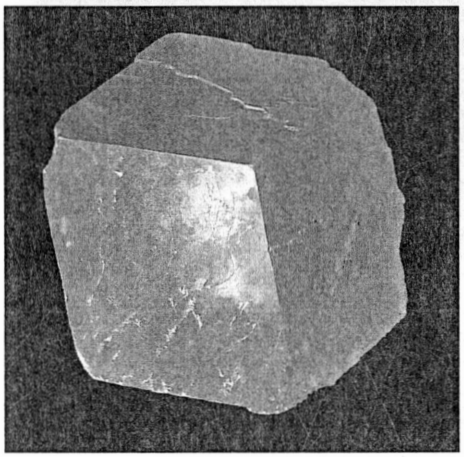

Calcite from Mrzen

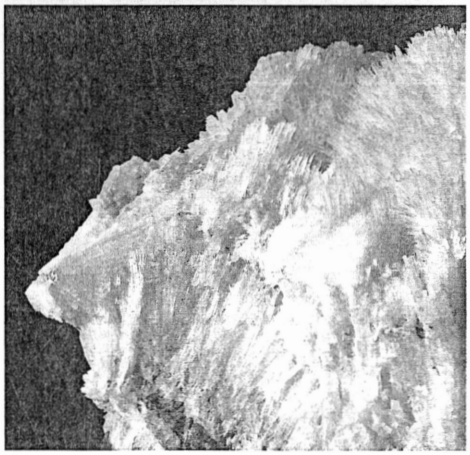

Aragonite from `Ržanovo

Siderite from Zletovo

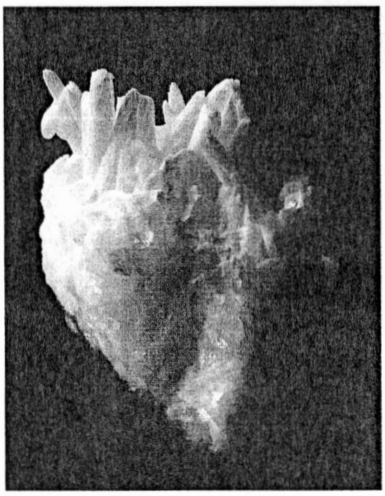

Kutnahorite from Sasa

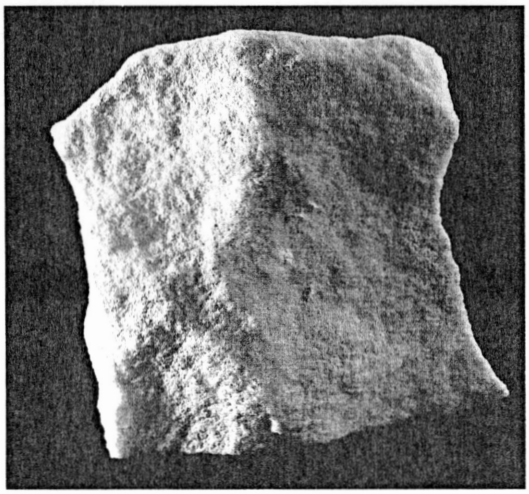

Dolomite from Prilep

Contributions, Sec. Math. Tech. Sci., **XXVI**, 1 (2005), pp. 7–84

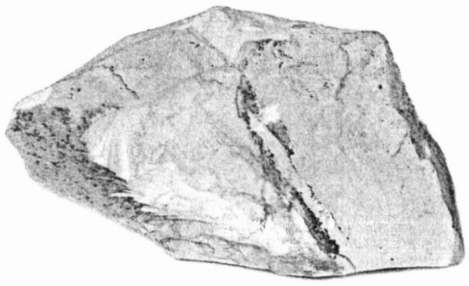

Magnesite from Pčinja

Galena from Sasa

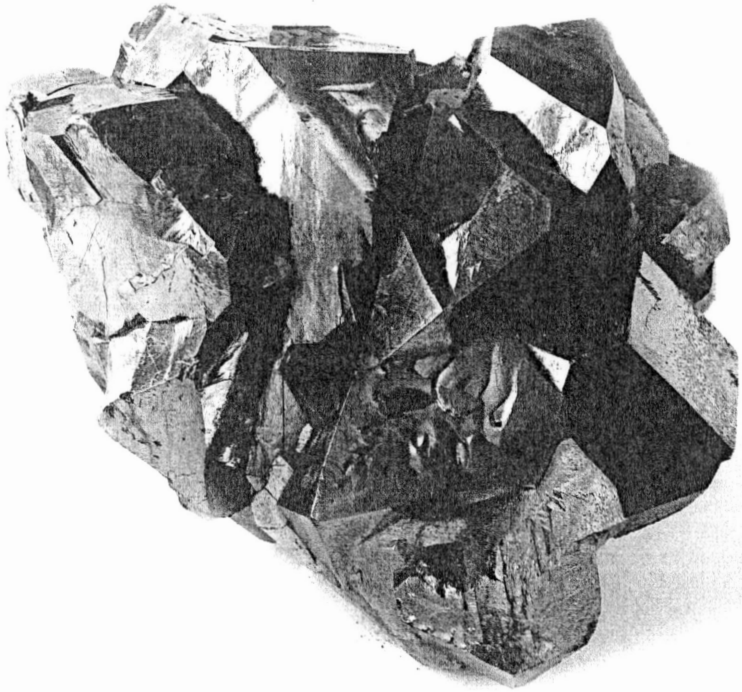

Galena from Zletovo

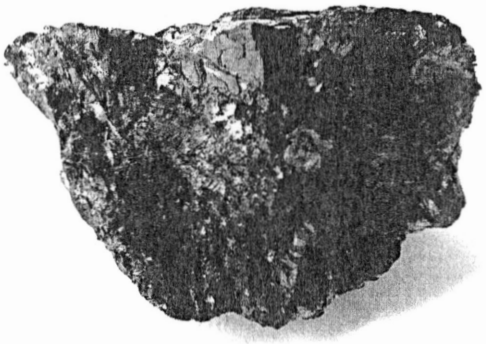

Sphalerite/Wurtzite from Zletovo

Sphalerite/Wurtzite from Toranica

Sphalerite/Wurtzite from Sasa

Hematite from Damjan

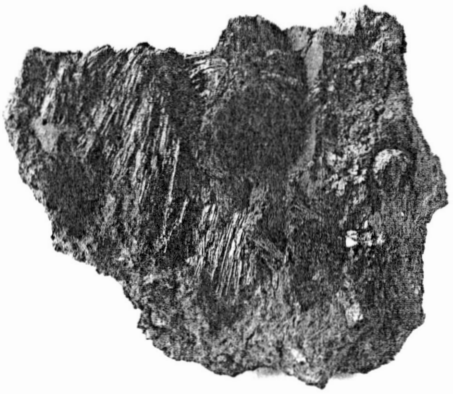

Hematite from `Ržanovo

Contributions, Sec. Math. Tech. Sci., **XXVI**, 1 (2005), pp. 7–84

Corundum from Sivec

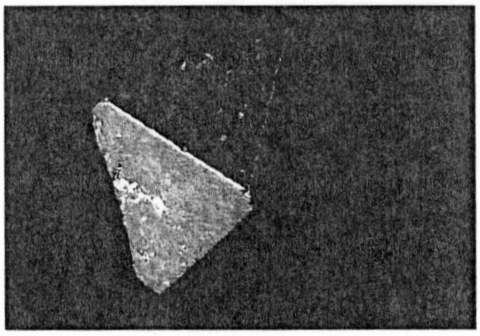

Magnetite from Košino

Magnetite from Damjan

Rutile from Veselčani

Chromite from Raduša

Прилози, Одд. мат. тех. науки, **XXVI**, 1 (2005), с. 7–84

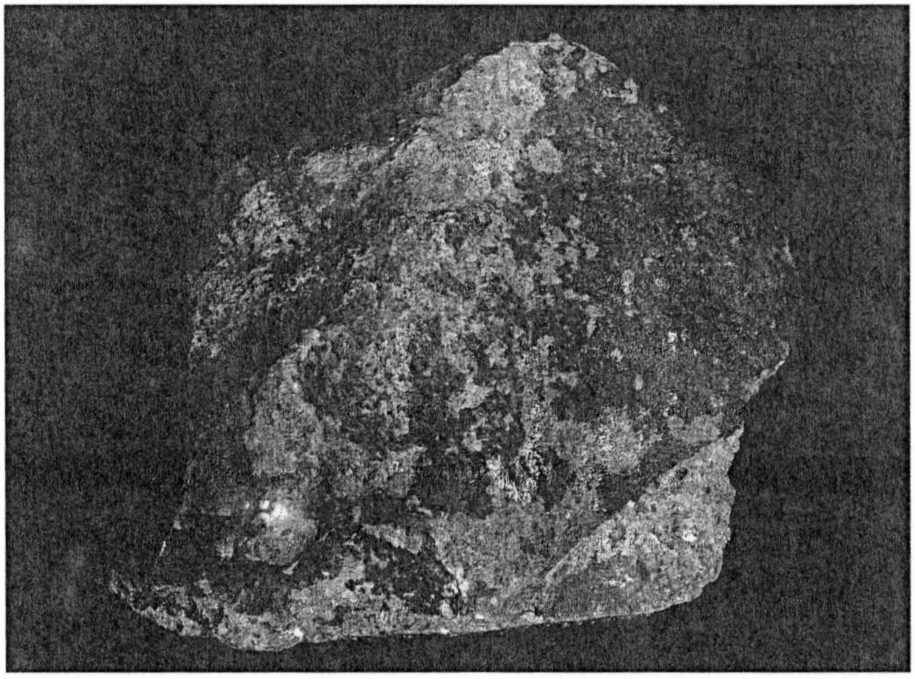

Limonite from Pehčevo

Goethite from Alšar

Olivine from `Ržanovo

Almandine from Pelagon

Zircon from Kozjak

Titanite from Dunje

Прилози, Одд. мат. тех. науки, **XXVI**, 1 (2005), с. 7–84

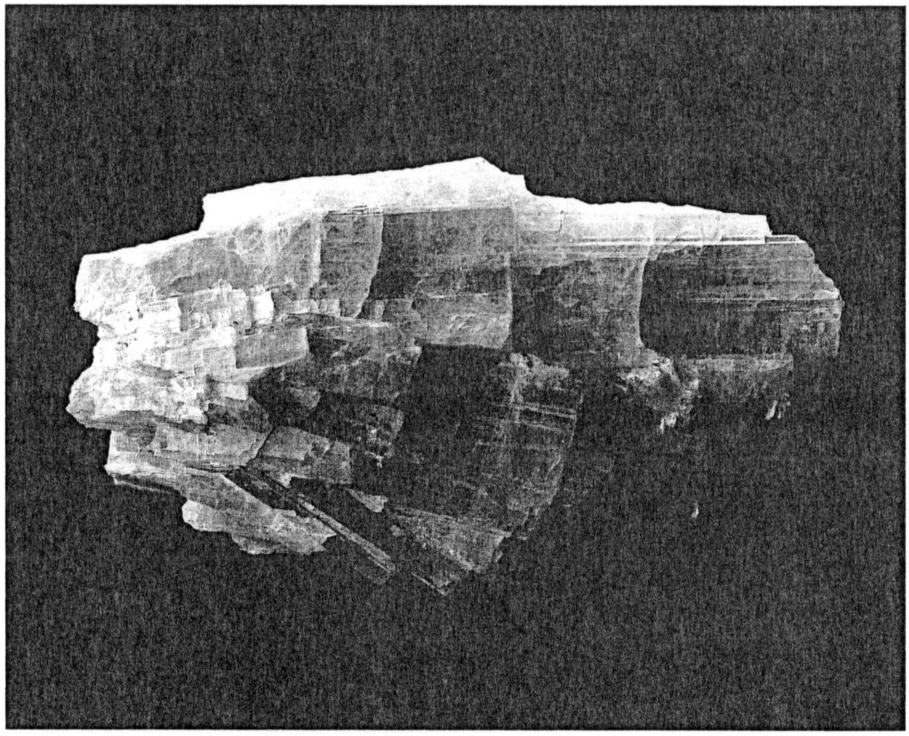

Kyanite from Štavica

Staurolite from Štavica

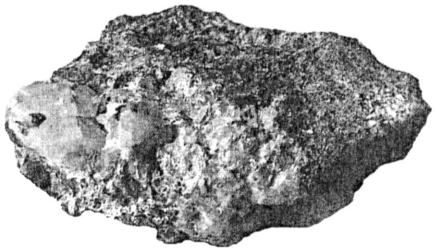

Spessartine from Lojane